EVALUATION OF SHEAR ENHANCEMENT FOR
HIGH-STRENGTH CONCRETE PLATES

GAIJU JIANG

NOTICE

AVIS

The quality of this microform is heavily dependent upon the quality of the original thesis submitted for microfilming. Every effort has been made to ensure the highest quality of reproduction possible.

La qualité de cette microforme dépend grandement de la qualité de la thèse soumise au microfilmage. Nous avons tout fait pour assurer une qualité supérieure de reproduction.

If pages are missing, contact the university which granted the degree.

S'il manque des pages, veuillez communiquer avec l'université qui a conféré le grade.

Some pages may have indistinct print especially if the original pages were typed with a poor typewriter ribbon or if the university sent us an inferior photocopy.

La qualité d'impression de certaines pages peut laisser à désirer, surtout si les pages originales ont été dactylographiées à l'aide d'un ruban usé ou si l'université nous a fait parvenir une photocopie de qualité inférieure.

Reproduction in full or in part of this microform is governed by the Canadian Copyright Act, R.S.C. 1970, c. C-30, and subsequent amendments.

La reproduction, même partielle, de cette microforme est soumise à la Loi canadienne sur le droit d'auteur, SRC 1970, c. C-30, et ses amendements subséquents.

Canadä

Evaluation of Shear Enhancement for High-Strength Concrete Plates

BY

© Dajiu Jiang, B.Sc. (Eng.)

A THESIS SUBMITTED TO THE SCHOOL OF GRADUATE
STUDIES IN PARTIAL FULFILLMENT OF THE
REQUIREMENTS FOR THE DEGREE OF
MASTER OF ENGINEERING

JANUARY 1994
FACULTY OF ENGINEERING AND APPLIED SCIENCE
MEMORIAL UNIVERSITY OF NEWFOUNDLAND
ST. JOHN'S   NEWFOUNDLAND   CANADA

Canada

To Danfeng Chao

Abstract

A research program including material investigation, experimental and analytical investigation on high-strength concrete plates are reported in this thesis.

Material investigation was carried out on the durability of high-strength concrete tensile properties under cold ocean environment (freeze-thaw cycles). Tensile properties of high-strength concrete in terms of modulus of rupture, direct tensile strength and fracture energy were examined up to 700 freeze-thaw cycles in laboratory simulated environment.

An experimental investigation on shear enhancement was carried out on seven high-strength concrete slabs to study the punching shear capacity and shear enhancement. Five types of different shear reinforcement, namely single bending, U-stirrup, double bending, shear-stud and T-headed shear reinforcement were tested and evaluated. The emphasis is placed upon the evaluation of their contribution to punching shear capacity of high-strength concrete plates. Structural behaviours were evaluated in terms of overall load-deflection response, ultimate loading capacity, post-ultimate loading capacity, ductility and energy absorption. Failure patterns and strain distribution were also discussed.

The analytical investigation was conducted by using the finite element analysis. The finite element analysis reported herein is an application of the nonlinear analysis of reinforced concrete structures using three-dimensional solid finite element. The purpose of this application is based on the fact that employing three-dimensional elements is the only successful way to model out-of-plane shear reinforcement in the

slabs. Hence, the three-dimensional twenty node brick element with 2×2×2 Gaussian integration rule over the element faces and a plasticity-based concrete model were employed in a finite element program. Single bending and double bending shear reinforcement were modeled with the smeared layer method, while shear-stud and T-headed shear reinforcement were depicted individually in the mesh. Reasonable agreement has been obtained between the numerically predicted behaviour and experimental test results. Transverse shear stress was evaluated by the finite element analysis in terms of punching shear, and compared with the unfactored punching shear resistance specified by the Canadian building design code.

Contents

List of Figures

List of Tables

List of Symbols

c/c	=	Reinforcement bar spacing from center to center
d	=	Slab effective depth
E_D	=	Dynamic modulus of elasticity
E_o	=	initial modulus of elasticity
h	=	slab thickness
n	=	positive direction normal to shell element reference surface
P_c	=	Relative dynamic modulus of elasticity
Q	=	lateral load at slab center
Q_u	=	ultimate lateral load at slab center
Q_y	=	lateral load at slab center when the first yielding occurred in the bottom flexure reinforcement
$Q_{\Delta u}$	=	lateral load associated with Δ_u at slab center
f_c	=	concrete compressive stress
f_r'	=	modulus of rupture
f_t	=	concrete tensile stress
f_t'	=	ultimate concrete tensile strength
ζ	=	natural coordinate of the three-dimensional brick element

η	=	natural coordinate of the three-dimensional brick element
ξ	=	natural coordinate of the three-dimensional brick element
ϵ_p	=	concrete plastic strain in a monotonically loaded uniaxial compression specimen
ϵ_y	=	Reinforcement steel yielding strain
Δ_y	=	deflection associated with the first yielding load Q_y at slab center
Δ_{Q_u}	=	deflection associated with the ultimate load Q_u at slab center
Δ_u	=	ultimate deflection at slab center in the post-ultimate loading capacity
D	=	deflection at slab center
U	=	ductility factor
τ_{ma^-}	=	maximum transverse shear stress from finite element analysis
v_r	=	unfactored punching shear resistance specified by the Canadian building design code
ρ	=	reinforcement steel ratio

Chapter 1

Introduction

With a fast development in the high-strength concrete industry, high-strength concrete flat plate has been widely used in building floors, bridge decks, long span structures, marine platforms and offshore structures in North America. Marine platforms and offshore structures frequently have a concrete perimeter wall which is normally designed to resist the impact of ice loads on the structure. Both flat and curved exterior walls have been used. Thus, the concrete plate represents one of the most predominant structural elements used in the walls of concrete offshore platforms. Currently, a gravity based structure utilizing high-strength concrete has been designed for the Hibernia Development off the eastern coast of Newfoundland.

The catastrophic nature of punching shear failure exhibited by reinforced plates in building floors, bridge decks and marine platforms when they were subjected to concentrated loads has been a major concern for engineers for many years. Placing suitable types of shear reinforcement in the high-strength concrete plate is an effective method to enhance punching shear capacity. The present building code specifications for shear strength of reinforced concrete plates are based on the test results of slabs with relatively low compressive strength and without shear resistance reinforcement.

1

Hence, there is a great need to understand the characteristics of the punching shear failure in the high strength concrete plate and to develop effective shear reinforcement to enhance its punching shear capacity.

1.1 Research scope

There are difficulties in examining the effects of cold ocean environment (freeze-thaw cycles) on the punching shear capacity of marine and offshore structures with a full-scale models. Concrete fracture energy and tensile strength have been considered as a sensitive material parameter correlative and directly related to punching shear failure (Bazant and Cao, 1987). Hence, the research program presented in this thesis includes a material investigation on high-strength concrete tensile properties under laboratory simulated freeze-thaw cycles, as an attempt to understand the punching shear behaviour. It has been recommended by Gustafsson and Hillerborg (1988) that the brittle nature of the punching shear behaviour indicates the close relation between the influence of fracture energy (tensile properties) and the punching shear strength.

An experimental and analytical investigation conducted on seven high-strength concrete slabs with five types of different shear reinforcement are reported in this thesis. The slabs with a column stub in this study are one-to-one full scale models of a typical prototype flat plate structure. The objectives of this phase in the thesis are to study the structural responses and to evaluate the shear enhancement of punching shear capacity of high-strength concrete plates.

The test slabs were simply supported along the four edges with corners free to lift. They were loaded transversely through a column stub at the centre by a hydraulic actuator in displacement control. The structural behaviour, the failure modes, strain

distribution and the shear enhancement of punching shear capacity of the slabs were observed and the test results and observation were analyzed.

A non-linear finite element (F. E.) analysis was carried out on these slabs as an analytical investigation. Three-dimensional twenty node brick element, and plasticity-based concrete model were implemented in a general purpose F. E. code, ABAQUS (Hibbitt et al, 1993), to perform F. E. analysis of the five slabs with different shear reinforcement. The previously developed two-dimensional F. E. model with eight node thick shell element (Marzouk and Chen, 1993) was used to perform F. E. analysis on two slabs without shear reinforcement. The discussion based on predicted-to-measured results was addressed in terms of ultimate load, deflection at the ultimate load, as well as transverse shear stress and its distribution.

1.2 Research objective

The main objectives of this investigation can be summarized as follows:

1. To investigate the tensile properties of high-strength concrete under freeze-thaw cycles.

2. To understand the effects of cold ocean environment (freeze-thaw cycles) on the punching shear strength of high-strength concrete marine and offshore structures, since it is directly related to tensile properties and fracture energy.

3. To investigate the punching shear behaviour of high-strength concrete plates with different types of shear reinforcement.

4. To evaluate the punching shear capacity of high-strength concrete plates in an attempt to make contribution to the relevant specification in building design

codes.

5. To provide a suitable finite element model for high-strength concrete slabs with different types of shear reinforcement in order to improve the relevant design procedure.

1.3   Thesis outline

Chapter 2 is a literature review of the recent research work relevant to the research topics. Chapter 2 is divided into three parts. The first part addresses the absence of information regarding the effects of the cold ocean environment (freeze-thaw cycles) on the tensile properties of high-strength concrete. The second part reviews previous research conducted on different types of shear reinforcement in concrete plates and addresses various design code specifications for shear strength of reinforced concrete slabs. The last part reviews the state-of-the-art in current non-linear finite element analysis of reinforced concrete structures. The application of non-linear finite element analysis in different reinforced concrete structures are selectively included.

Chapter 3 presents the material investigation phase of this research. The effects of freeze-thaw cycles on high-strength concrete tensile properties are discussed in terms of modulus of rupture, direct tensile strength, post cracking behaviour and fracture energy.

Chapter 4 decribes the experimental test set-up for test slabs. Design of shear reinforcements, details of experimental facilities, test procedures and instrumentation are presented.

Chapter 5 presents the test results and observations obtained from the experimental investigation as well as the analysis of these results.

Chapter 6 presents the finite element modeling of the test slabs, and the predicted-to-measured results are discussed.

Finally, a summary of the investigation and conclusions reached are given in Chapter 7.

Chapter 2

Review of Literature

2.1 Investigation of high-strength concrete properties

A recent development in the high-strength concrete industry has been to use fly ash and silica fume as partial replacements for portland cement in the production of high-strength concrete. The new high-strength concrete has been used in North America for tall buildings, bridges, long span structures and marine structures, and it is also being used for offshore platforms. Compressive strengths of 70 to 120 MPa have been produced easily in the field with materials and equipment normally used in the concrete industry. Compressive strength-cost analysis revealed that the concrete producer could realize important savings by using silica fume in the concrete mixture. Various properties of high-strength concrete examined were reviewed in an ACI special report (ACI Committee 363, 1992).

Concrete properties such as stress-strain relationship, modulus of elasticity, tensile strength, shear strength, and bond strength were examined in terms of the uniaxial compressive strength of 152×305 mm cylinders. Axial-stress versus strain curves for concrete compressive strength up to 83 MPa were obtained by Shah et al (1981). A

6

simple method of obtaining a stable descending portion of the stress-strain curve was described by Wang et al (1978). High-strength concrete exhibits less internal micro-cracking than lower-strength concrete for a given imposed axial strain (Carrasquillo et al, 1981).

Recently, it is increasingly evident that tension properties of concrete has become a major factor contributing to nonlinear behavior of reinforced concrete structures. Tension properties of concrete governs its cracking behaviour which was previously ignored or treated in a very approximate way in the design and analysis. An accurate analysis of load-deflection characteristics, crack width, bond transfer and shear transfer is based on the post-cracking response of concrete. In addition, the concrete tensile strength has been considered as a sensitive material parameter correlative with punching shear failure (Bazant and Cao, 1987). Therefore, there is a great need for information in this area. The investigation of tension properties of high-strength concrete has been carried out at M.U.N. in an ongoing research program. Uniaxial tensile stress-strain curves including softening response of high-strength concrete and fracture energy has been obtained (Chen, 1993).

Very little information is available on the effect of freeze-thaw cycles in cold ocean environment on the tension properties of high-strength concrete. Freeze-thaw cycles pose a serious problem for concrete structures in cold ocean environments. Previous research has been carried out on the durability of high-strength concrete with regard to the chemical aspects of concrete durability, the resistance to freezing and thawing, and the corrosion of reinforcing steel (Mehta, 1991). Previous investigations conducted on the effect of freezing and thawing on tension properties of high-strength concrete have only been focused on relative dynamic modulus, volume change, com-

pressive strength, capillary absorption, and porosity of high-strength concrete (Whiting and Burg, 1991; Maage and Helland, 1991; Malhotra et al, 1988). The present investigation on high-strength concrete tensile properties under laboratory simulated freeze-thaw cycles has been carried out at M.U.N. (Marzouk and Jiang, 1993b)

2.2 Shear enhancement of punching shear capacity of concrete slabs

2.2.1 Introduction

Reinforced concrete slabs without drop panels can be used to represent flat plates in building floor system, which is supported by columns without capitals. The slab also can be employed to simulate the bridge deck and/or the structural element subjected to concentrated impulsive loading in marine and offshore structures.

Particularly in the building floor system, the reinforced concrete flat plate is an economical and popular structural system. It is popular in construction because it is easy to form and construct. A disadvantage of this type of structure is the great risk of the brittle punching failure at the slab-column connection. A number of methods including considering different types of shear reinforcement were developed to solve this problem (Broms, 1990; Mortin and Ghali, 1991; Alexander and Simmonds, 1992). A great deal of research has been done on developing efficient types of shear reinforcement in concrete slab (ASCE-ACI Joint Committee 426, 1974). A comprehensive overview of experimental investigation on various types of shear reinforcement to enhance punching shear capacity of concrete slabs is reviewed in this section. Also, various proposed approaches adopted by different building design codes to predict the punching shear capacity of the concrete slabs with shear reinforcement are provided

in this section.

2.2.2 Experimental evaluation of different types of shear reinforcement

2.2.2.1) Nature of the problem

In addition to limiting deflection under service loads, the greatest practical problem of flat plate systems is punching shear failure at the slab-column connection region. The catastrophic nature of the punching shear failure exhibited by reinforced concrete flat plates when subjected to concentrated loads has concerned engineers for many years. In many cases, the design of flat plate structures is governed by the punching shear capacity of the structure.

"Punching failure" is associated with a particular collapse mechanism in which the column and an attached portion of slab push through the slab. The slab breaks along a sloping surface that extends from the compression side of the slab at the face of the column to the tension side of the slab at some distance from the column. Failure referred to as punching failure is of particular concern because of its catastrophic consequences. The so-called punching shear failure of slabs without shear reinforcement occurs suddenly without warning so that, normally, no remedial measures can be applied prior to failure. Several such failures have been reported in the literature (Dilger and Ghali, 1981).

In the past, several papers have addressed the punching shear resistance of flat-slabs without shear reinforcement (Elstner and Hognestad, 1956; Vanderbilt, 1972; ASCE-ACI Joint Committee 426, 1974 and Regan, 1984). These papers discuss the effect of concrete strength, flexural reinforcement, shear span, and test method. Later,

various solution have been attempted to prevent punching-shear failures. These range from simply using a thicker slab or column capitals in the critical zones to providing various types of shear reinforcement.

If the design of a slab is found to be adequate for flexure, but not for punching shear, and an increase of the depth in the whole is not desired, four possibilities exist to increase the shear strength: (1) increase the slab thickness in the vicinity of the column (provide a drop panel); (2) if this is not enough, flare the top of the column (i.e., use a column capital); (3) use of higher concrete strength; and (4) provide shear reinforcement. In many cases drop panels and column capitals are unacceptable architecturally. Therefore, when a shear capital or a drop panel is not used, at the same time, the slab depth is limited, only leave the combination of high concrete strength and the practically efficient shear reinforcement as possible alternatives for many structures.

2.2.2.2) Experimental investigations on different types of shear reinforcement

Provision of shear reinforcement can increase the shear capacity of a slab-column connection to a value higher than the theoretical flexural capacity according to Johansen's yield line theory. There have been many attempts to develop shear reinforcement for slabs. It was, however, recognized that shear reinforcement for slabs creates special problems because of relatively small slab thickness. ACI Committee 318 (1989) recognizes that the effectiveness of shear reinforcement depends on its anchorage, even though it may be difficult to achieve in thin and medium-thickness slabs. In additional, labour cost resulting from complicated placement of shear reinforcement is of

considerable importance in practical design.

More recently, studies have been conducted to verify the effect of shear reinforcement. Various types of shear reinforcement including bent bars, stirrups (closed or U type), shearheads (I- or C-channel structural steel sections placed in the slab around the column), welded wire fabric, studs, hat-shaped shear reinforcement and hooked bars were evaluated. These types of shear reinforcement are summarized in a number of excellent papers (Corley and Hawkins, 1968; Seible et al, 1980; Yamada et al, 1992). It was shown that effective shear reinforcement can improve both punching shear resistance and ductility (ACI Committee 318, 1989). Tests have been established that to be fully effective, 1) shear reinforcement is required to intercept shear cracks and to prevent their widening and 2) the anchorage must be capable of developing yield strength of the shear reinforcement (ACI Committee 421, 1992).

Dilger and Ghali (1981) claimed that the use of bent-up bars as shear reinforcement was first investigated by Graf, Elstner and Hognestad, Franz, Anderrson, Rosenthal and Yitzhaki. Closed and open stirrups were tested by Franz, Wantur, Carpenter, Keefe and Narasinham. Shearhead cages were used by Moe, Anderson and Leonhardt. Shearheads consisting of structural steel plates or structural steel sections, or both, were investigated by Hawkins (1974a). Welded wire fabric were evaluated by Dilger and Ghali (1981), and Broms (1990). The so called shear stud was developed by Ghali, and reviewed in a great deal numbers of his papers (Seible et al, 1980; Mokhtar et al, 1986; Elgabry and Ghali, 1990; Mortin and Ghali, 1991). It consists of studs mechanically anchored at each end by a plate or head capable of developing the yield strength of the studs. Hat-shaped shear reinforcement and hooked bars were examined by Yamada et al (1992).

In many of these tests it has been found that the shear reinforcement consisting of bent-bars is not fully effective, which means that it does not reach the yield strength at failure. The reason is that the anchorage of the bent bars or stirrups is not sufficient to develop the full capacity of the bars. In case of bent-up bars, the tensile force in the inclined leg is associated at the bends with compressive stresses higher than the concrete strength and with a pull-out effect of the horizontal portion of the bar. This leads to an increase in the width of the shear crack, which when extending to the compression zone results in the failure of compression resistance before the shear reinforcement reaches its yield capacity.

Similar observations have been made on stirrups. A 90 degree bend at the end of a vertical stirrup generates high concrete compressive stresses under the bend and also has a certain pull-out effect of the horizontal leg under high stress in the vertical leg. The slip observed in experiments explains why it is difficult or, perhaps, impossible to develop the yield strength of the stirrups. The need for special care for anchorage details for shear reinforcement in slabs has been emphasized by many researchers. In order to make normal stirrups reasonably effective, Hawkins (1974a), Langohr et al (1976), Seible et al (1980) and Yamada et al (1992) recommended to enclose the top and bottom flexural reinforcement. For this reason, the installation of these stirrups in situ is a time-consuming job, and it is virtually impossible in thin slabs with 150-200 mm thickness. Also, the welded wire fabric did not behave satisfactorily unless placed in a specific way which would complicate construction.

Experimental results from the investigation by Yamada et al (1992) showed that the hat-shaped shear reinforcement was not effective because of lack of proper anchorage and large spacing. Double-hooked reinforcement showed high effectiveness, which

resulted in a considerable increment of punching shear resistance of the connection. However, installation of double-hooked reinforcement is time-consuming.

In recognition of these problems, the ACI Building Code Requirements for Reinforced Concrete (ACI Committee 318, 1989) permit the use of shear reinforcement in the form of bars, as in the vertical legs of stirrups. The ACI Committee 318 (1989) commentary emphasizes the importance of anchorage details of the shear reinforcement and accurate placement, especially in thin slabs (ACI Committee 421, 1992). However, punching shear resistance of flat-slab systems is addressed even more restrictively in other building codes, such as the one presently enforced in Japan (Architectural Institute of Japan, 1988), which dose not allow any contribution of shear reinforcement. Therefore, there is great need for more information available to evaluate the contribution of various types of shear reinforcement.

2.2.3 Different building code requirements for shear reinforcements

The American Concrete Institute Code (ACI Committee 318, 1989), the Canadian Code (CSA A23.3-M84, 1984), the Australian Code (AS3600, 1988) as well as the British Code (BS 8110, 1985) will be reviewed in this section in the area about design and placement of shear studs and stirrups specified to the two-way slab. The Japanese Code (Architectural Institute of Japan, 1988) dose not allow any contribution of shear reinforcement and the other code requirements in Europe are quite vague in this area. Therefore, they are not included in this review. Current building codes relating to shear reinforcement in two-way slabs are empirically based. Shear reinforcement has taken many forms. The basic principle involves placing steel reinforcement in such a manner that it will take a specified portion of the total applied shear force within the

connection.

2.2.3.1) The American Concrete Institute Code (ACI Committee 318, 1989)

According to ACI Committee 318 (1989) recommendations, punching shear capacity must be satisfied at a critical section perpendicular to the plane of the slab. The critical section is located so that its perimeter b_0 is minimum, but must not be closer than a distance of $d/2$ to the column face. Design of the critical section of slab should be based upon

$$v_u \le \phi v_n \tag{2.1}$$

in which v_u is the shear stress in the critical section caused by the factored load transfer between the slab and the column, v_n is the nominal shear stress, and ϕ is the strength reduction factor equal to 0.85. It should be highlighted that the ACI code dose not include the material factors for steel and concrete which are becoming more important in other codes. A factored shear capacity is accomplished by using this *strength reduction* factor (equal to 0.85 for shear). The *overloads* factors employed in the ACI Code has a dead load factor of 1.4 and a live load factor of 1.7.

The nominal shear stress v_n can not exceed $4\sqrt{f_c'}$ (psi) if shear reinforcement is not used. The normal shear stress v_n is limited to a maximum of $6\sqrt{f_c'}$ (psi) when shear reinforcement is used. Even when the so-called shearhead is used, the maximum normal shear stress is $7\sqrt{f_c'}$ (psi). The shear reinforcement must be designed to carry all shear stress in excess of $2\sqrt{f_c'}$ (psi). When shear reinforcement is considered in the slab, the shear capacity at the critical section shall be computed by

$$v_n = v_c + v_s \qquad (2.2)$$

in which

$$v_c = 2\sqrt{f_c'} \qquad (2.3)$$

and

$$v_s = \frac{A_v f_{yv}}{b_0 s} \qquad (2.4)$$

where A_v is the cross-sectional area of the vertical types of shear reinforcement on one peripheral line parallel to the perimeter of the column section and s is the spacing between peripheral lines of the vertical shear reinforcement. The code also suggests that the shear reinforcement should be as symmetrical as possible about the centroid of the critical section in the location, number and spacing of the stirrups. This also applies at edge columns although the shear stresses are concentrated towards the front face of the column. This helps to reinforce against torsional stresses in the strip of the slab along the free edge.

The shear reinforcement has taken many forms in different building design codes. The ACI Code recognizes the following types of shear reinforcement for beams and slabs:

1. Stirrups perpendicular to the plane of the slab.

2. Welded wire fabric with wires perpendicular to the plane of the slab.

3. Stirrups at an angle great than forty-five degrees to the longitudinal tension reinforcement.

4. Longitudinal reinforcement with the bent portion making an angle greater than or equal to thirty degree with the longitudinal reinforcement.

5. Combinations of stirrups and bent steel reinforcement.

6. Spirals.

7. Shear heads.

The problems with these types of reinforcement when used for slabs were summarized by Dilger and Ghali (1981). Shear reinforcement consisting of bars is not fully effective, with the steel not reaching yield at failure, when the anchorage of the bent bars or stirrups is insufficient to develop the full capacity of the bars. In the case of bent-up bars, the tensile force in the inclined legs is associated with compressive stress higher than the concrete strength and with a pull-out effect in the horizontal portion of the bar. Similar effects have been shown in stirrups in the tests. Vertical slips exceeding 1 mm have been observed in beam shear tests. In slabs, this slip can make it difficult, if not impossible, to develop the yield strength. Significant anchorage slip in shear reinforcement consisting of welded wire fabric was also observed by Seible (1980). It is difficult and time-consuming to install flexural steel in the slab when complicated stirrups are used. Shear heads are quite expensive and may interfere with the column steel to make it difficult to place. In thin slabs shear heads cannot be used at all due to limited space.

2.2.3.2) The Canadian Code (CSA A23.3-M84, 1984)

The Canadian Code up until 1984 is a quite close copy of the ACI Code. The CSA A23.3-M84 (1984) has been adjusted to reflect a greater concern with material

uncertainties. The dead and live load factors have been reduced to 1.25 and 1.50 respectively. The strength reduction factors dealing with failure mechanisms have been removed and replaced with material factors ϕ_c equal to 0.6 for concrete and ϕ_s equal to 0.85 for reinforcement steel. The design rules in the CSA C23.3-M84 (1984) specify that the maximum factored shear force, V_f, due to the factored load transfer between the column and the slab shall be investigated at a critical section located at a minimum distance but not closer than 0.5 d to the column face, and at successive sections more distant from this face. The maximum shear force, V_f, shall not exceed the factored shear resistance, V_r. When shear reinforcement is not provided, the factored shear resistance, V_r, shall not be greater than the factored shear capacity of concrete, V_c, where

$$V_c \leq 0.4\lambda\phi_c\sqrt{f'_c}b_0 d \tag{2.5}$$

If shear reinforcement is provided, the factored shear resistance, V_r, shall not exceed $0.6\lambda\phi_c\sqrt{f'_c}b_0 d$, and should be calculated by

$$V_r = V_c + V_s \tag{2.6}$$

in which

$$V_c \leq 0.2\lambda\phi_c\sqrt{f'_c}b_0 d \tag{2.7}$$

and

$$V_s = \frac{\phi_s A_v f_y d}{s} \tag{2.8}$$

where A_v is the cross-sectional area of the vertical types of shear reinforcement on one peripheral line parallel to the perimeter of the column section and s is the spacing between peripheral lines of the vertical lines of shear reinforcement.

The Canadian code recognizes the use of bars, wires, shear heads and a type of reinforcement investigated at University of Calgary (Dilger and Ghali, 1981). This reinforcement, with a brand name of Studrail currently, consists of Nelson type studs with shafts welded to round anchor heads, with an area greater than or equal to ten times the area of the stud at the top, and to a steel strip at the bottom. Holes are drilled in the strip so that it may be easily attached to the formwork using screws or nails. This type of shear reinforcement has several advantages over those discussed above in thin slabs. They are relatively inexpensive to manufacture and install. CSA A23.3-M84 (1984) also recommends the shear reinforcement design rules developed by Dilger and Ghali (1981).

2.2.3.3) The Australian Code (AS3600, 1988)

The traditional types of shear reinforcement was moved away from the Australian Code. The method using closed stirrups to reinforce against shear and torsion on the side face of connections subjected to unbalanced moments has been taken into consideration. Having been based initially on the ACI code however, the use of shear heads is still permitted. Shear studs are acceptable but no real provision is given for design.

2.2.3.4) The British Code (BS 8110, 1985)

The British Code at present refers only to bent-up bars and shear links as acceptable reinforcement. The implementation of shear combs was only suggested as an acceptable form of shear reinforcement in some recent design proposal.

2.3 Nonlinear finite element analysis of concrete structures

2.3.1 Introduction

Punching shear failures of concrete plates follow a fairly predictable sequence. Various classical methods based on empirical or rational studies has been used to predict the ultimate loading capacity of concrete slabs in punching shear failure in past several decades (Graf, 1930; Richart and Kluge, 1939; Forsell and Holemberg, 1946 and Hognestad, 1953). Hawkins (1974b) grouped existing analytical models for predicting punching shear failure of slab-column connections into three categories. They include:

1. Models based on linear distribution of shear stress on some critical section. This is perhaps the simplest approach and is favored by most design codes.

2. Models based on beam analogies. Beam analogies describe a slab-column connection as the junction of orthogonal beam elements contained within the slab.

3. Models based on plate theory.

A general analytical model for a slab-column connection should predict both the ultimate capacity of the connection and the mechanisms by which load is carried. It is, however, recognized that each model contains elements that are not consistent

with observed behavior. On the other hand, efforts to predict punching failure on the basis of some limiting strain criteria so far have not been successful (Van Dusen, 1985).

With the development of numerical techniques in recent years, there are capability and reliability to develop accurate numerical models suitable for normal-strength or high-strength concrete in order to reflect punching shear behaviour. In this section, the state-of-the-art for nonlinear finite element analysis of reinforced concrete structures are reviewed. The current application of nonlinear analysis in concrete structures are, also, reviewed.

2.3.2 Nonlinear analysis of reinforced concrete structures

2.3.2.1) The importance of nonlinear analysis

The reasons for nonlinear analysis are that 1) concrete tensile softening behaviour after cracking can be described, 2) nonlinear material stress-strain constitutive relationship can be modeled, and 3) concrete properties including creep, shrinkage and time-dependent changes can be reflected.

Results from nonlinear finite element analysis of reinforced concrete structures are dependent on the stress-strain relationship and failure criteria used for 1) modeling concrete, steel reinforcement and the steel-concrete interface (bond and dowel actions), 2) modeling of cracking and post-cracking behaviour of reinforced concrete (including aggregate interlock, dowel action, and tension stiffening effects), and 3) the type of finite element and the size of mesh used to idealize the structure.

2.3.2.2) Constitutive relationship and failure criteria

An extensive review of the stress-strain constitutive modes yielded over the past two decades was undertaken by the ASCE-ACI Joint Committee on Finite Element Analysis of Reinforced Concrete Structures (ASCE, 1982), Chen (1982) and Shareef and Buyukozturk (1983). The available modes are called, namely, a) elastic-based models including linear elastic model, nonlinear elastic (total secant) model and incremental (hypoelastic) model; b) plasticity-based models including elastic perfectly plastic model and elastic hardening plastic model; c) plastic fracturing model; d) endochronic theory model; and e) boundary surface model. Highlights of these constitutive relationships for concrete and the advantages and disadvantages of these models are reviewed in an excellent paper by Bahlis et al (1987). Two distinct failure criteria among a number of failure criteria were incorporated in the most modern computer programs. The failure criterion for plain concrete under biaxial loadings was proposed by Tasuji et al (1976), and modified further by Al-Mahaidi (1979). The failure criterion based on reinforced concrete under biaxial tensile-compressive stresses was proposed by Vecchio and Collins (1982).

2.3.2.3) Cracking and post-cracking behaviour of concrete

Cracking of concrete is one of the important sources of material nonlinearity in reinforced concrete members. Because of the difficulty to account for continued propagation of cracks with increase in loading, the smeared cracking model is currently employed in the analysis. The so-called smeared cracking model is based on the concept of stress discontinuity while maintaining displacement continuity. When the principal tensile strain in an element exceeds a predefined value, many finely spaced

cracks are assumed to form in the plane perpendicular to the maximum principal tensile strain direction (Tasuji et al. 1976).

After concrete has cracked, three phenomena, namely, aggregate interlock, dowel action, and tension stiffening, are incorporated in the nonlinear analysis in order to satisfy the modeling of the post-cracking behaviour. The descending branch of the tensile stress-strain curve of concrete is incorporated in modeling the tension stiffening effect (Marzouk and Chen, 1993).

2.3.2.4) Idealization of reinforcement

In the present analysis, the steel reinforcement is treated as a uniaxially stressed material distributed over the element in any direction. A composite concrete-steel constitutive relationship is derived for the element, based on the assumption that perfect bond exists between the steel and the concrete (Bahlis and Mirza, 1987).

2.3.2.5) Numerical solution technique for concrete nonlinear analysis

In a nonlinear analysis for concrete collapse problem, several numerical solution techniques can be used. In this research work, a numerical solution technique, named as automatic control of time stepping, is used. When a step and certain tolerance are defined, the increments to model the step are automatically selected in this method. The automatic incrementation assumes that convergence will occur relatively smoothly as the iterations progress, so that the number of iterations needed to achieve convergence to the specified tolerances can reasonably be predicted from the rate at which the residuals are reduced from one iteration to the next during the early iterations (Hibbit et al, 1993).

2.3.3 Application of finite element analysis of reinforced concrete structures

The non-linear finite element analysis of reinforced concrete members and structures has been applied more and more widely in practical design and analysis. A number of general survey or state-of-the art papers (Bergan and Holand, 1979; Schnobrich, 1974; Schnobrich, 1977; Schnobrich, 1978; Scordelis, 1972; Scordelis, 1978; and Wegner, 1976) have been written on the finite element analysis or reinforced concrete structures which contain numerical results for examples. In this section, the review will only focus on typical examples of numerical applications for shallow and deep beams, shear resistance walls and panels, two-way slabs, axisymmetric solids, and general three-dimensional solids.

2.3.3.1) Shallow beam and deep beam

For shallow beams failing in shear and for deep beams, where inclined cracking under combined stress states occur, the beam was modeled as a two-dimensional plane stress system. Discrete cracks or distributed cracks were modeled with various assumptions for material behaviour and reinforcement model (Grootenboer, 1979; Ngo et al, 1967). A typical finite element analysis of two shallow beams with simple support was presented by Cedolin and Dei Poli (1977). An example of finite element study on deep beams was given by Buyukozturk (1977).

2.3.3.2) Shear panels and walls

Cervenka and Gerstle (1971) were the first to make a finite element investigation of several shear panels which they had tested experimentally. A variety of finite element

models and material laws has been used in these analyses (Agrawal et al. 1976; Darwin and Pecknold, 1976). A typical analysis of a three story shear wall subjected to six cycles of load reversals was presented by Agrawal (1977). Agrawal also presented a dynamic analysis of the same wall using a time history input of earthquake induced ground accelerations.

An international competition was organized to compare analytical methods for predicting the response of reinforced concrete elements subjected to general two-dimensional stress states. Cervenka's was the best finite element model of several models conducted to investigate four shear panels tested experimentally at University of Toronto in the international competition (Collins et al, 1985).

2.3.3.3 Two-way slabs under center point load

A corner supported slab under center point load was first studied experimentally and analytically by Jofriet and McNiece (1971). This example has been subsequently used by many others (Bashur and Darwin, 1978; Hand et al, 1973; Kabir and Scordelis, 1979 and Lin and Scordelis, 1975). Subsequent analyses of the same slab have used triangular or quadrilateral finite elements, nonlinear biaxial constitutive relations and failure theories, as well as various assumptions for the tension stiffening effect.

Recently, an ongoing research program carried out at Memorial University of Newfoundland has been conducted on the high-strength concrete slabs simply supported along all four edges and loaded transversely through a stub-column at the center of the slab (Marzouk and Chen, 1993 and Marzouk and Jiang, 1993a). A plasticity-based concrete model was used for the finite element analysis. An eight-node quadrilateral shell element with a reduced 2 x 2 Guassian integration over the

element plane and nine-point Simpson-type integration over the element thickness were employed. A suitable post-cracking tensile model of reinforced high-strength concrete was utilized based on the fracture energy of high-strength concrete recorded from stress-displacement curves (stress-crack width curves). In this research, a new finite element model implementing a three-dimensional element with a reduced 2 x 2 x 2 Guassian integration rule over the element faces was developed to predict the punching shear behaviour of high-strength concrete slabs with different types of shear reinforcement.

2.3.3.4) Axisymmetric analysis of a prestressed concrete reactor vessel (PCRV)

A strong impetus to the development of solutions for axisymmetric solids has been in connection with reinforced and prestressed concrete reactor vessels. These structures involve great expenditures of money and must be designed under the most stringent design criteria. General papers dealing with the nonlinear finite element analysis of these structures have been published by Zienkiewicz et al (1971), as well as others. Several examples were given by ASCE (1982) in a comprehensive paper on PCRV analyses.

Between 1975 and 1980 a research program to investigate the static overpressure response of Gentilly-2 type secondary containment structures was undertaken at the University of Alberta for the Atomic Energy Control Board of Canada. Later, a program named FEPARCS5 (Finite Element Program for the Analysis of Axisymmetric Reinforced and Prestressed Concrete Structures) was developed by Elwi and Murray (1984).

2.3.3.5) Three-dimensional analysis of a prestressed concrete reactor vessel (PCRV)

Applications of the nonlinear analysis of reinforced concrete structures using three-dimensional finite elements have been limited to date, primarily because of the large computer times and costs involved. An example of three-dimensional analysis of a prestressed concrete reactor vessel (PCRV) was detailed by Connor and Sarne (1975).

Chapter 3

Freeze-and-Thaw Effects on Shear Strength & Tensile Properties of High-Strength Concrete

3.1 Introduction

Freeze-thaw cycles pose a serious problem for concrete structures in cold ocean environments. It is very difficult to examine the punching shear capacity of high-strength concrete marine platforms and offshore structures weakened by freeze-thaw cycles with a full scale structural specimen. However, Bazant and Cao (1987) considered that punching shear strength are significantly correlated to concrete tensile properties. Hence, the material investigation conducted on a number of designed high-strength and normal strength concrete specimens is presented in this chapter in order to obtain the information in this area. The experimental investigation focused on the effect of freeze-thaw cycles on the fracture energy and tension properties of high-strength concrete compared with normal strength concrete. Experimental tests consisted of measuring the relative dynamic modulus of elasticity, the modulus of rupture, the direct tensile strength and the change in mass of air entrained concrete specimens.

A special effort was devoted to determine the fracture energy and the post-cracking response after 700 cycles of exposure to freezing and thawing. Specimens of normal strength concrete were used as reference specimens.

3.2 Experimental investigation

3.2.1 Materials

In this investigation, local materials were utilized, based on the recommendations of an earlier investigation (Marzouk and Hussein, 1989) and test results obtained by Marzouk and Hussein (1990) at the concrete laboratory of Memorial University of Newfoundland (M.U.N.). The destination compressive strength of the 28th day was designed to reach 70 MPa for high-strength concrete, and 35 to 40 MPa for normal strength concrete, respectively. Ordinary portland cement (Type 10) as produced in Newfoundland was used. A 12% replacement of cement by fly ash (Type F) (ASTM, 1991a) and an 8% replacement by silica fume were used on the basis of mass. Chemical and physical analyses of the portland cement, the fly ash and the silica fume used in the experiment are given in Tables 3.1 and 3.2. The local coarse aggregate consisted mostly of crushed quartzite sandstone with a minor fraction of siltstone and shale. It had a maximum nominal size of 20 mm for the standard prisms and 10 mm for the direct tension specimens. Local fine aggregate which had a similar composition to the coarse aggregate was used. The fine aggregate consisted mainly of quartzite sandstone with a fineness modulus of 3.1. A neutralized vinsol resin air-entraining agent, a non chloride water reducing agent of polyhydroxy-carboxylic base and a superplasticizer of sulphonated naphthalene formaldehyde base were also used in the mix. The mix proportions of high-strength and normal strength concrete are given

in Table 3.3. Normal strength concrete were used as a reference specimen for the high-strength concrete specimen.

3.2.2 Test specimens

Relative dynamic modulus of elasticity

Two sets of high-strength and normal strength concrete (75×75×350 mm) prisms were prepared for measuring pulse velocity and resonant frequency in order to obtain the relative dynamic modulus of elasticity of concrete. Each set consisted of 12 specimens. The specimens were cast and cured for 28 days in accordance with ASTM (1991b). Nine high-strength concrete specimens and nine normal strength concrete specimens were placed into the freeze-thaw apparatus at the same time. The rest of the specimens were kept as reference specimens in the high humidity curing room. Three companion standard cylinders were cast with each mix for the determination of the compressive strength.

Modulus of rupture

After the relative dynamic modulus of elasticity test was completed for 700 cycles, two additional sets of high-strength and normal strength concrete (75×75×350 mm) prisms were prepared for modulus of rupture tests. Each set consisted of 24 specimens and three companion standard cylinders for compressive strength. Eighteen high-strength concrete specimens were placed into the freeze-thaw apparatus. Three specimens were kept as reference specimens in the high humidity curing room, and three others were tested to find the modulus of rupture before cycling. The same procedure was repeated for normal strength concrete.

Table 3.1: Chemical analysis of portland cement and supplementary cementing materials

Description of Test	CSA Type 10 †Cement	Fly Ash	Silica Fume
Chemical Analysis,%			
SiO_2	20.89	44.93	95.41
Al_2O_3	4.38	27.79	1.09
Fe_2O_3	3.20	19.06	0.00
CaO	60.28	0.92	0.32
MgO	3.71	1.44	0.73
Na_2O	0.35	0.82	–
K_2	0.15	0.54	0.61
SO_3	4.01	0.43	0.24
Mn_2O_3	–	0.67	–
Loss of Ignition	2.04	2.88	1.80
Total	100.0	99.48	99.20
$SiO_2 + Al_2O_3 + Fe_2O_3$	–	91.80	–
Potential Compound Composition, %			
C_4AF	9.43		
C_3A	6.36		
C_3S	40.17		
C_2S	29.59		
$C_3 + C_2S$	69.75		

† As manufactured in Newfoundland

Table 3.2: Physical analysis of portland cement and supplementary cementing materials

Description of Test	CSA Type 10 †Cement	Fly Ash	Silica Fume
Physical Tests–General			
Time of set (Vicat Needle, min.,)			
Initial	120		
Finial	220		
Fineness: -45 μm	96.2		
Blaine Surface Area m^2/kg	425.0		
% retained on 45 μm by wet sieving		14.5	
Fineness m^2/kg			20,000
Water Requirement, %		92.0	139
Pozzolanic Activity Index with:			
Portland Cement at 28-d, %		99.0	119.1
Lime, MPa		6.7	12.5
Physical Tests-Mortar Compressive Strength, MPa			
3-d	24.09		
7-d	27.17		
28-d	37.17		

†As manufactured in Newfoundland

Table 3.3: Mix proportions per cubic metre of concrete

Mix design	High-strength concrete	Normal strength concrete
Cement	400 *kg*	350 *kg*
Fly Ash	60 *kg*	—
Silica Fume	40 *kg*	—
Cement, Fly Ash & Silica Fume	500 *kg*	350 *kg*
Fine Aggregate	600 *kg*	700 *kg*
†Coarse Aggregate	1,000 *kg*	1,200 *kg*
Air Entraining Agent	250	300 *ml*
Water Reducing Agent	750 *ml*	1,400 *ml*
Superplasticizer	8000 *ml*	1500 *ml*
W/C	—	0.45
W/(C+Fa+Sf)	0.30	—
Properties of fresh concrete		
Slump	100 *mm*	120 *mm*
Air Content	3.80%	4.2%
Density	2410 *kg/m³*	2290 *kg/m³*

† The coarse aggregate had a maximum nominal size of 20 mm
for the standard prisms (75x75x350 mm), and a nominal size
of 10 mm for the thin direct tension specimens (20x75x300 mm)

Direct Tension Test

Two sets of high-strength and normal strength concrete were prepared for casting the direct tension (20×75×300 mm) specimens. Each set consisted of 12 specimens, and three companion standard cylinders for compressive strength. The direct tension specimens were cast in a special plexiglass mold built at M.U.N.. The fresh concrete was placed into the molds, and a vibrating table was used for compacting. The specimens were covered with saturated burlap for 24 hours at room temperature, and were immersed in water to cure for 28 days. The specimens were notched on both edges. The notches were cut by a circular diamond concrete saw with notch dimensions of 11 mm in depth and 3 mm in width.

3.2.3 Apparatus

A freeze-thaw test apparatus meeting the requirement of ASTM (1991c) was used, consisting of 18 chambers in which specimens were completely surrounded by water. The freeze-thaw cycle consisted of alternately lowering the temperature of the specimens from 18.3 to -17.8 °C and raising it from -17.8 to 18.3 °C in 3.4 hours.

Direct tension tests were conducted on the test set-up developed in an earlier investigation at M.U.N. (Chen, 1993) The test system consisted of a closed-loop servohydraulic universal test machine, a pair of special wedge-type frictional grips, and a high-speed data acquisition system. The grips permit a uniform transfer of shear stress to the concrete specimen. An electromechanical extensometer (gauge length of 25 mm) was used to control the loading. Cracking was initiated from the centre of the specimen by providing notches as described above. The deformation across the notch was measured by the extensometer (mounted across the notch), and

transformed into electric signal fed back to the servocontroller to control the loading. The gauge length of 25 mm was based on the assumption that the cracking process zone of a direct tension specimen is 2.5 times the maximum nominal aggregate size (10 mm). The ratio of a cracking process zone to the maximum nominal aggregate size fell into the normal range of 1.5 to 4.0 for various types of concrete as recommended by Bazant and Oh (1983). The strain, converted from the measured deformation, was equal to the deformation divided by the gauge length (25 mm) as mentioned before. The strain and the load data were simultaneously logged into the X-Y Recorder (Hewlett Packard, Model 7046 A) and a data acquisition system (System 200, from Sciemetric Instruments Inc.)

3.2.4 Test Procedure

The dimensions, pulse velocity, longitudinal resonant frequency and the mass of each specimen were determined before placing the specimens in the freeze-thaw apparatus. Each specimen was placed in a metal container manufactured at M.U.N.. Standard concrete prisms were surrounded by 3 mm of water inside a ($84 \times 84 \times 430$ mm) metal container, while the thin tension specimens were surrounded by 5 mm of water inside a ($30 \times 90 \times 430$ mm) metal container.

Specimens were removed for tests when they were in a thawed condition at 100 cycle intervals. The masses, resonant frequencies and pulse velocities were recorded. Before returning specimens to the freeze-thaw apparatus in a random order, containers were cleaned out and fresh water was added.

At every 100 cycle interval, a minimum of three standard ($75 \times 75 \times 350$ mm) concrete prisms were tested for modulus of rupture in accordance with ASTM (1991d).

A minimum of two direct tension test ($20 \times 75 \times 300$ mm) specimens were tested also at 100 cycle intervals.

All the concrete specimens were exposed up to 700 freeze-thaw cycles. It should be noted that 700 freeze-thaw cycles far exceeds the limit of 300 cycles set by ASTM (1991c).

3.3 Experimental observation and discussion

3.3.1 Relative Dynamic Modulus of Elasticity and Modulus of Rupture ($75 \times 75 \times 350$ mm prisms)

The high-strength concrete prisms showed small loss of mass after 700 freeze-thaw cycles, while normal strength concrete prisms showed considerable loss of mass as shown in Table 3.4. The resonant frequency was measured in the longitudinal direction, while the travel time for the ultrasonic pulse velocity was measured in the transverse direction. Normally, the transverse measurement would give less accurate reading than the longitudinal measurement, since the longitudinal measurement has a longer time travel, which results in less error due to resolution of time measurement. An average value of three readings was obtained in the transverse direction to gain a more accurate result. A typical specimen during the measurement of resonant frequency is shown in Fig 3.1.

The average values of the relative dynamic modulus of elasticity from resonant tests after 300, 500 and 700 cycles were 88%, 85% and 83% for high-strength concrete, and 73%, 61% and 45% for normal strength concrete, respectively. The relative dynamic modulus of elasticity for some of the high-strength and normal strength concrete prisms versus the number of freeze-thaw cycles is shown in Figs 3.2 and 3.3.

Table 3.4: Mass and change of mass in percent of standard concrete prisms (75×75×350 mm)

specimens	Mass (g) at different cycles					†Change of mass (%) at different cycles				
	0	200	300	500	700	0	200	300	500	700
H 1	5204	5192	5192	5184	5171	0.0	-0.2	-0.2	-0.4	-0.6
H 2	5163	5158	515i	5143	5121	0.0	-0.1	-0.2	-0.4	-0.8
H 3	5121	5121	5124	5116	5102	0.0	0.0	!0.0	-0.1	-0.4
H 4	5112	5123	5126	5117	5109	0.0	+0.2	+0.3	+0.1	-0.1
H 5	5094	5091	5093	5085	5071	0.0	-0.1	-0.0	-0.2	-0.4
H 6	5110	5088	5085	5076	5063	0.0	-0.4	-0.5	-0.7	-0.9
H 7	5236	5217	5216	5207	5197	0.0	-0.4	-0.4	-0.5	-0.7
H 8	5063	5059	5050	–	–	0.0	-0.1	-0.3	–	–
H 9	5277	5277	5268	–	–	0.0	0.0	-0.2	–	–
N 1	4308	4295	4281	4250	4250	0.0	-0.3	-0.6	-1.3	-2.4
N 2	4331	4285	4268	4233	4181	0.0	-1.1	-1.4	-2.3	-3.5
N 3	4250	4250	4261	4258	4175	0.0	0.0	+0.3	+0.2	-1.8
N 4	4228	4195	4170	4116	4069	0.0	-0.8	-1.4	-2.7	-3.8
N 5	4267	4275	4278	4227	4225	0.0	+0.2	+0.3	-0.9	-1.0
N 6	4302	4298	4302	4262	4218	0.0	-0.1	0.0	-0.9	-2.0
N 7	4337	4302	4304	4216	4210	0.0	-0.8	-1.0	-2.8	-2.9
N 8	4240	4240	4226	4195	4193	0.0	0.0	-0.3	-1.1	-1.1
N 9	4326	4313	4299	4268	4262	0.0	-0.3	-0.6	-1.3	-1.5

† – indicates loss in mass: + indicates gain in mass

36

Figure 3.1: Standard Concrete prism (75 × 75 × 350 mm) during resonant frequency test

A severe deterioration in normal strength concrete was obvious after 500 cycles, as shown in Figs 3.4.

A summary of the modulus of rupture test results is given in Table 3.5. Each reading represents the average value of three specimens. The normal strength concrete showed more severe strength loss after 700 cycles of freezing and thawing than the high-strength concrete. The average modulus of rupture of normal strength concrete after 700 cycles was only 40% of its original average value before cycling. For high-strength concrete, the average modulus of rupture was 85% of the corresponding value before cycling.

Both of the relative dynamic modulus of elasticity and the modulus of rupture results reflected the severe deterioration of the normal strength concrete beyond 300 cycles and the good performance of the high-strength concrete. The good durability of high-strength concrete can be attributed to its low permeability and higher compressive strength (Mehta, 1991).

It is important to point out that the strength gained in high-strength concrete during the first six months is much more than that of normal strength concrete. Calcium silicates (C-S-H), calcium aluminates, and calcium hydroxide are products of the normal hydration process. Also, the hydrated products contain some quantities of unhydrated cement and water in both evaporable and nonevaporable forms. Calcium hydroxide, a by-product of cement hydration, reacts at room temperature with the silica fume and fly ash to form tobermorite gel, which has a very stable and strong cementing quality. This pozzolanic reaction contributes to the large increase in strength for high-strength concrete during the first six months. After 700 cycles, concrete has had about four and half months to mature (4 weeks for curing
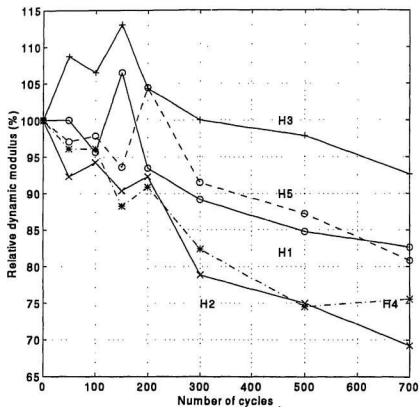
Figure 3.2: Relative dynamic modulus of elasticity versus number of cycles for standard high-strength concrete prisms (75×75×350 mm)
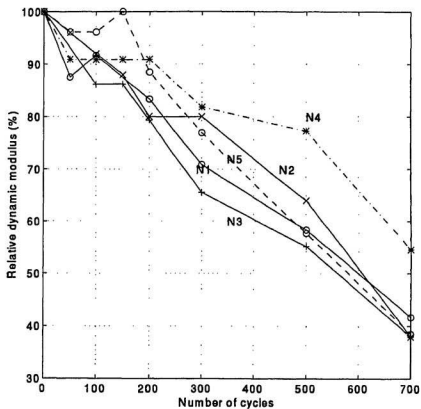
Figure 3.3: Relative dynamic modulus of elasticity versus number of cycles for standard normal strength concrete prisms (75×75×350 mm)

High-Strength Concrete
H5
(500 Cycles)

Normal Strength Concrete
N5
(500 Cycles)

Figure 3.4: Standard concrete prisms showing greater amount of surface damage in normal strength concrete (75 × 75 × 350 mm) after 500 cycles

Table 3.5: Modulus of rupture values after freeze-thaw cycles

No. of specimens	No. of cycles	Modulus of rupture f_r (MPa)		Standard deviation of f_r (MPa)	
		normal	high	normal	high
3	0	5.47	6.57	0.57	0.46
3	100	4.40	6.36	0.42	0.63
3	200	4.10	6.00	0.63	0.49
3	300	3.80	5.98	0.32	0.51
3	400	3.62	5.70	0.69	0.32
3	600	2.99	5.69	0.55	0.56
3	700	2.19	5.60	0.48	0.48

and 14 weeks for cycling). Therefore, it is expected that during the cycling process, high-strength concrete gains more strength due to the pozzolanic reaction.

3.3.2 Tension specimens (20×75×300 mm)

The changes in mass of the thin direct tension specimens are given in Table 3.6. It is clear from the table that the change in mass of high-strength concrete specimens was less than 1%, compared with 8% for normal strength concrete. The fundamental longitudinal resonant frequencies of both high-strength and normal strength concrete specimens are shown in Table 3.7. A typical thin direct tension specimen during measurement of the longitudinal resonant frequency is shown in Figure 3.5. The average relative dynamic modulus of elasticity, based on resonant frequencies after 300, 600 and 700 cycles was about 82%, 69% and 66%, respectively, for the high-strength concrete specimens. The corresponding values for normal strength concrete were 72%, 54% and 39%, respectively. The dynamic modulus of elasticity was calculated from the measured ultrasonic pulse velocity across the 20 mm transverse dimension by using the relationship between pulse velocity and dynamic modulus of elasticity, provided by the manufacturer of the instrument. These calculated values are given in Table 3.8. It is noted that these values are approximate because the dynamic modulus of elasticity is related to the density and Poisson's ratio, which were not determined. The average value of relative dynamic modulus of elasticity for high-strength concrete specimens after 300, 600 and 700 cycles was 77%, 68% and 65% respectively. The corresponding values for normal strength were 71%, 45% and 39%, respectively.

The results of the resonant frequency and the pulse velocity tests were similar and indicated that high-strength concrete was more durable than normal strength

Table 3.6: Mass and change of mass in percent of thin direct tension concrete specimens (20×75×300 mm)

specimens	Mass (g) at different cycles								† Change of mass (%) at different cycles							
	0	100	200	300	400	500	600	700	0	100	200	300	400	500	600	700
H 1	1142	1140	–	–	–	–	–	–	0.0	-0.2	–	–	–	–	–	–
H 2	1084	1083	–	–	–	–	–	–	0.0	-0.1	–	–	–	–	–	–
H 3	1106	1107	1105	1104	1107	1102	1102	1100	0.0	0.0	-0.1	-0.2	0.0	-0.4	-0.4	-0.5
H 4	1105	1104	1104	1103	1105	1102	1102	1097	0.0	-0.1	-0.1	-0.2	0.0	-0.3	-0.3	-0.7
H 5	1179	1179	1179	1178	1181	1175	1176	1175	0.0	0.0	0.0	-0.1	+0.2	-0.3	-0.3	-0.3
H 6	1063	1063	1062	1061	1064	1060	–	–	0.0	0.0	-0.1	-0.2	+0.1	-0.3	–	–
H 7	1073	1072	1072	1070	1072	1070	1070	–	0.0	-0.1	-0.1	-0.3	-0.1	-0.3	-0.3	–
H 8	1149	1149	1148	1144	1148	1144	1144	1143	0.0	0.0	-0.1	-0.4	-0.1	-0.4	-0.4	-0.5
H 9	1129	1128	1130	1128	–	1125	–	–	0.0	-0.1	+0.1	-0.1	–	0.4	–	–
H10	1106	1105	1105	1103	1107	1104	1103	–	0.0	-0.1	-0.1	-0.3	–	-0.2	-0.3	–
H11	1220	1220	1218	–	–	–	–	–	0.0	0.0	-0.2	–	–	–	–	–
N 1	976	969	959	934	925	912	911	907	0.0	-0.7	-1.7	-4.3	-5.2	-6.6	-6.7	-7.1
N 3	989	980	967	954	949	945	943	935	0.0	-0.9	-2.2	-3.5	-4.0	-4.4	-4.7	-5.5
N 4	981	981	969	956	973	943	940	940	0.0	–	-1.2	-2.5	-0.8	-3.9	-4.2	-4.2
N 5	961	957	948	930	950	920	917	914	0.0	-0.4	-1.4	-3.2	-1.1	-4.3	-4.6	-4.9
N 6	999	993	985	967	985	957	954	951	0.0	-0.6	-1.4	-3.2	-1.4	-4.2	-4.5	-4.8
N 7	960	952	943	909	924	887	885	881	0.0	-0.8	-1.8	-5.3	-3.7	-7.6	-7.8	-8.2
N 8	991	987	969	946	965	937	934	933	0.0	-0.4	-2.2	-4.5	-2.6	-5.4	-5.8	-5.9
N 9	977	966	963	947	967	938	938	930	0.0	-1.1	-1.4	-3.1	-1.0	-4.0	-4.0	-4.8
N10	1021	1011	1009	989	1008	976	971	968	0.0	-1.0	-1.2	-3.1	-1.3	-4.4	-4.9	-5.2
N11	1016	1009	998	982	999	968	962	960	0.0	-0.7	-1.8	-3.3	-1.7	-4.7	-5.3	-5.5
N12	1023	998	1010	990	1008	979	975	975	0.0	-2.4	-1.3	-3.2	-1.5	-4.3	-4.7	-4.7

† – indicates loss in mass; + indicates gain in mass

Table 3.7: **Resonant frequencies and the relative dynamic modulus of elasticity for tension specimens (20×75×300 mm)**

specimens		Longitudinal resonant frequencies n (Hz) at different cycles								Relative dynamic modulus of elasticity (%) at different cycles		
		0	100	200	300	400	500	600	700	300	600	700
High-strength	H 1	2496	2490	–	–	–	–	–	–	–	–	–
	H 2	2535	2513	–	–	–	–	–	–	–	–	–
	H 3	2529	2520	–	2112	2115	1924	1915	1902	69.7	57.3	56.6
	H 4	2445	2442	2436	2390	2143	2154	2136	2014	95.6	76.3	67.9
	H 5	2510	2574	2537	2574	2199	2089	2167	2161	–	74.5	74.1
	H 6	2359	2107	2377	2430	2076	2114	–	–	–	–	–
	H 7	2791	2689	2446	2386	2293	2218	2169	–	73.1	60.4	–
	H 8	2474	2360	2467	2271	2404	2169	2147	1997	84.3	75.3	65.2
	H 9	2505	2505	2501	2454	2234	2195	–	–	96.0	–	–
	H10	2503	2499	2489	2100	2742	2241	2068	–	70.4	68.3	–
	H11	2618	2609	2592	–	–	–	–	–	–	–	–
Normal strength	N 1	2449	2400	2421	1980	1787	1650	1693	1635	65.4	47.8	44.6
	N 3	2582	2501	2498	2321	2051	2001	1967	1821	80.8	58.0	49.7
	N 4	2866	–	2875	2268	1653	1613	2047	1757	62.6	50.7	37.3
	N 5	2382	–	2385	1935	1423	1906	1856	1477	66.0	60.7	38.4
	N 6	2904	2715	1919	2388	2233	2395	2084	1575	67.6	51.5	29.4
	N 7	2664	2575	2426	2716	1557	2373	1770	–	–	44.1	–
	N 8	2915	2466	1985	2383	1724	1893	1882	1553	66.8	41.7	28.4
	N 9	2622	2587	1990	2361	1657	2563	2043	1857	81.1	60.7	50.2
	N10	2500	2403	1980	2266	–	2285	1977	1528	82.2	62.5	37.4
	N11	2428	2210	1993	2391	1462	2770	1977	1594	97.0	66.3	43.1
	N12	2934	2111	2256	2096	1852	2109	2087	1644	51.0	50.6	31.4

Table 3.8: The relative dynamic modulus of elasticity using ultrasonic pulse velocity for tension specimens (20×75×300 mm)

Specimen		Dynamic modulus, E_D (GPa) across 20 mm direction at different cycles								Relative dynamic modulus of elasticity P_c (%) at different cycles		
		0	100	200	300	400	500	600	700	300	600	700
High-strength	H 1	55	39	–	–	–	–	–	–	–	–	–
	H 2	49	37	–	–	–	–	·	–	–	–	–
	H 3	53	–	41	41	41	38	37	36	77.4	69.8	67.9
	H 4	58	38	40	38	41	39	37	35	65.5	63.8	60.3
	H 5	48	36	40	34	33	35	32	30	70.8	66.7	62.5
	H 6	58	41	–	54	47	44	–	–	93.1	–	–
	H 7	58	36	44	53	52	48	43	–	91.4	74.1	–
	H 8	54	38	44	44	37	38	37	37	81.5	68.5	68.5
	H 9	52	38	38	38	37	37	–	–	73.1	–	–
	H10	54	36	36	36	36	34	35	–	66.7	64.8	–
	H11	36	31	30	–	–	–	–	–	–	–	–
Normal strength	N 1	34	32	26	24	20	17	14	14	70.6	41.2	41.2
	N 3	38	34	25	25	21	19	18	16	65.8	47.4	42.1
	N 4	37	29	25	23	19	16	15	12	62.2	40.5	32.4
	N 5	35	33	27	25	21	21	17	14	71.4	48.6	40.0
	N 6	39	36	28	26	22	18	16	12	66.7	41.0	30.8
	N 7	29	27	25	21	15	12	–	–	72.4	0.0	0.0
	N 8	39	32	25	22	19	18	16	13	56.4	41.0	33.3
	N 9	35	26	26	23	20	17	15	11	65.7	42.9	31.4
	N10	28	25	25	23	21	18	18	15	82.1	64.3	53.6
	N11	37	32	26	25	19	15	14	11	67.6	37.8	29.7
	N12	39	35	26	26	22	20	18	15	66.7	46.2	38.5
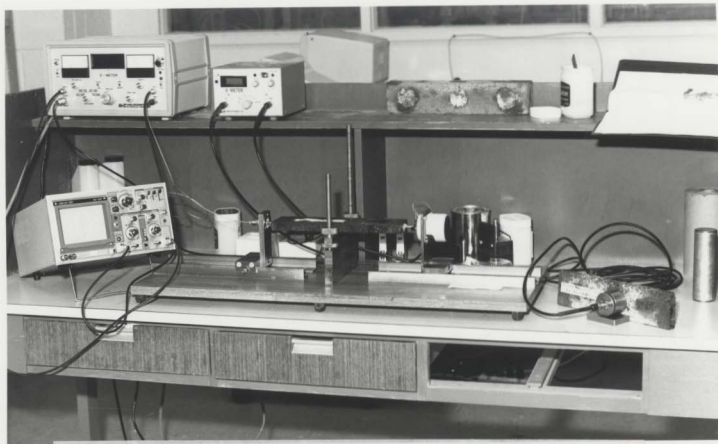
Figure 3.5: Thin direct tension high-strength concrete specimen (20 × 75 × 300 mm) during measurement of longitudinal resonant frequency

concrete. It should be noted that the direct tension specimens showed slightly more and faster deterioration than the standard freeze-thaw prisms due to the smaller thickness of the tension specimens, since the thickness of the direct tension specimens was 20 mm compared with 75 mm for the standard freeze-thaw prisms. The surface deterioration of a typical thin direct tension specimen of high-strength and normal strength concrete after 600 cycles is shown in Figs 3.6 and 3.7.

The tension specimens were tested using an (MTS) loading frame equipped with specially designed, wedge-type, frictional grips (Chen, 1993). The average values reported in Table 3.9 include direct tensile strength (f_t') and its corresponding strain (ϵ_p), initial modulus of elasticity (E_0) and compressive strength (f_c'). The direct tensile strength (f_t') is defined as the ultimate stress on the stress-strain curve, and its corresponding strain (ϵ_p) is named the cracking strain. The initial modulus of elasticity (E_0) is defined as the secant modulus at the stress of $0.45 f_t'$.

The test results of the reference high-strength concrete specimens before cycling presented in Table 3.9 were recorded by Chen (1993) in a previous study. Specimens HS1, HS3, and HS4 were identical in dimension and mix design to the direct tension specimens used for this investigation. The compressive strength of the three cylinders tested in Chen's investigation had an average value of 74.2 MPa. The compressive strength for three high-strength concrete cylinders used for this investigation had an average value of 69.4 MPa.

The present test results indicated that for high-strength concrete the direct tensile strength after 700 cycles of freezing and thawing was only 74% of the original value. The average value of the strain (cracking strain) corresponding to maximum stress after 100, 500 and 700 cycles was 83, 92 and 65$\mu\epsilon$ respectively. A minimum of two
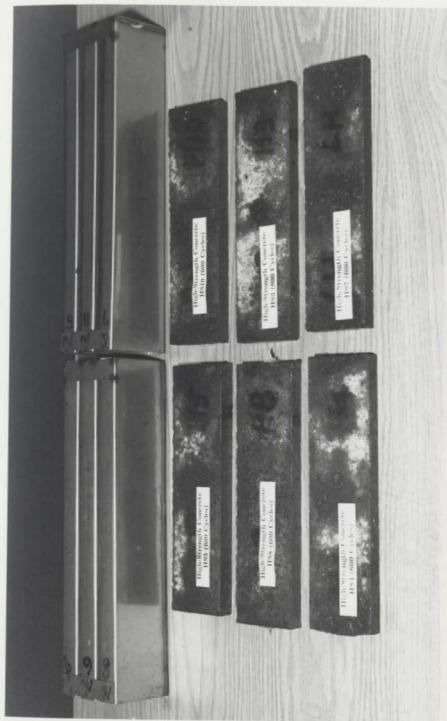
Figure 3.6: Thin direct tension high-strength concrete specimens (20 × 75 × 300 mm) after 600 cycles
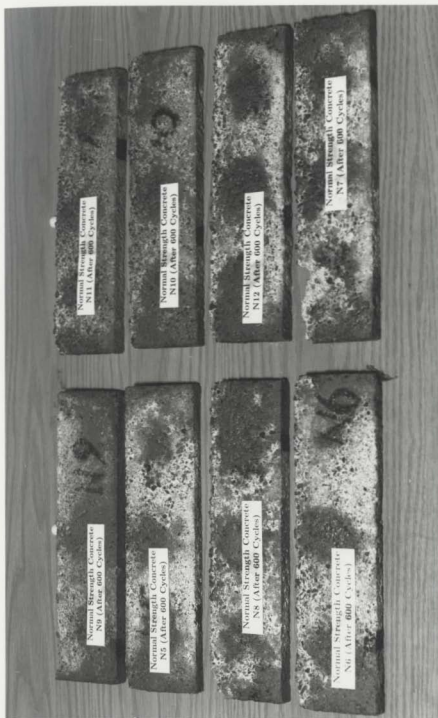
Figure 3.7: Thin direct tension normal strength concrete specimens (20 × 75 × 300 mm) after 600 cycles

Table 3.9: Direct tension test results after freeze-thaw cycles for high-strength concrete specimens (20×75×300 mm)

			Direct tension tests			
			Average value			
Cycles	f_c' MPa	Specimen 20×75×300 mm	f_t' MPa	$\epsilon_p \times 10^6$ $\mu\epsilon$	$E_0 \times 10^3$ MPa	f_t'/f_c' (%)
0†	74.2	HS1, HS3, HS4	3.15	115	48.6	4.2%
100	69.4	H 1, H 2	2.68	83	32.2	3.9%
200	69.4	H11	1.61	50	32.2	2.3%
500	69.4	H 6, H 9	2.70	92	29.4	3.7%
600	69.4	H 7, H10	2.66	93	28.5	3.6%
700	69.4	H 3, H 4, H 5	2.33	65	33.1	3.4%

† Adoported from a previous research program (Chen, 1993)

tension tests were performed at 100, 500 and 600 cycles. Before cycling and at 700 cycles, a minimum of three specimens were used. The direct tensile strength was 4.2% of the compressive strength before cycling. After 700 cycles, the direct tensile strength was 3.4% of the compressive strength.

3.3.3 Strain softening and fracture energy after 700 cycles

The post-cracking behavior and fracture energy of concrete are significant for an accurate stress analysis of a structural member. The fracture energy is needed to determine the punching shear strength based on a nonlinear fracture mechanics model often called the factious model (Gustafsson and Hillerborg, 1988). The complete tensile stress-strain curves for high-strength concrete specimens before cycling and after 700 cycles are shown in Fig 3.8. The effect of 700 cycles of freezing and thawing was evident on the stress-strain curve. The ascending portion of the stress-strain diagram indicated more brittle behavior with a smaller maximum stress and smaller inelastic strain. The descending portion of the curve descended more sharply after the peak stress. The strain energy density (area under stress-strain curve for concrete in tension) can be related directly to the fracture energy as detailed by Massicotte et al (1990). The integration of the area under the tensile stress-strain curve was conducted up to a strain value of 16 ϵ_p, which is defined as the maximum effective tensile strain. The associated fracture energy of high-strength concrete was calculated to be 5.7 and 3.5 times of the area under the ascending portion of their complete stress-strain curves before cycling and after 700 cycles respectively. The strain energy density of high-strength concrete after 700 cycles was about 70% of the original value before cycling.
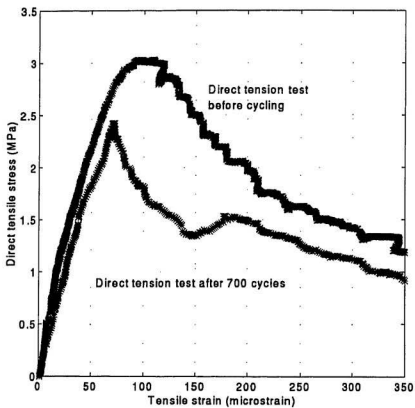
Figure 3.8: Stress-strain curve for high-strength concrete specimens under direct tension before and after 700 freeze-thaw cycles

Chapter 4

Experimental Investigation on Test Slabs

4.1 Introduction

One of the main objective of this research work is to investigate the punching shear mechanism of high-strength concrete plates with different types of shear reinforcement, and to evaluate the shear enhancement on punching shear capacity of high-strength concrete plates in an attempt to make a contribution to the relevant specification in building design codes.

The test program consisted of testing and evaluating the structural performance of seven high-strength concrete slabs. Five slabs with different types of shear reinforcement were tested. Two slabs with no shear reinforcement were tested as reference specimens. All slabs were designed to yield a ductile shear failure as detailed by Marzouk and Hussein (1991). The ductile shear failure mode can be characterized by yielding of the tension steel in a certain area around the column stub before punching occurs. One test set-up was used for all of the specimens utilizing different equipment to measure the deformations and strains through the testing program.

4.2 Test slabs

The test slabs had a side dimension of 1,950 mm and were simply supported along all four edges with corners free to lift. The load was applied transversely through a stub-column. The stub-column was cast monolithically at the centre of the slab. The slab extended 60 mm beyond the centre of the support. The dimensions and reinforcement details of the slabs are shown in Figs. 4.1 to 4.9 and Table 4.1. The slab-column connections tested in this study are one-to-one full scale model of a typical prototype flat plate structure. The specimen can also represent the region of r .gative bend moment around an interior column and the simply supported edges simulate the lines of contraflexure (Marzouk and Hussein, 1991).

The test variables of the study included five different types of shear reinforcement. They are named as single bend, U-stirrups, double bend, shear-stud and T-headed shear reinforcement. Test slabs were classified into Series I and II. Slabs in Series I including the reference specimens of Slab HS17 and HS19 with bottom reinforcement only and no diagonal shear reinforcement. Slab HS17 had a reinforcement ratio of 1.093, a bar size of 15 mm and a bar spacing of 166 mm centre to centre. Slab HS19 was designed with the same reinforcement ratio but with different reinforcement arrangement, i.e. a bigger sized bar (20mm) and greater spacing between bars (266 mm centre to centre).

The slabs in Series II included Slab HS18, HS20, HS21, HS22 and HS23 were designed with five different types of shear reinforcement to evaluate their contribution to the punching shear behaviour. The shear reinforcement of Slab HS18 consisted of five single bend (10 mm) bars placed at the central area of the slab with a spacing of 150 mm centre to centre in each direction. Slab HS20 had 10 mm U-stirrup shear

56
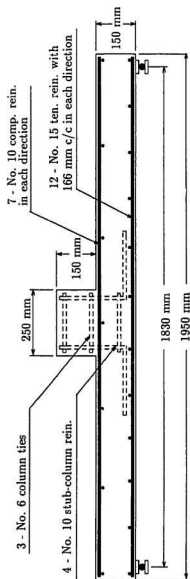
Figure 4.1: Dimension and reinforcement details of a reference slab (HS17)
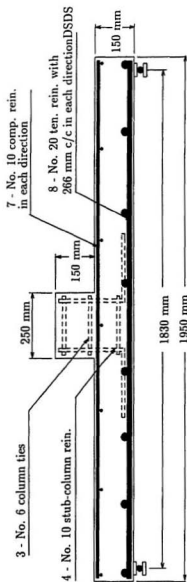
Figure 4.2: Dimension and reinforcement details of a reference slab (HS19)

Detail of single bend shear reinforcement

365 mm

365 mm

90 mm

48°

45°

250 mm

3 - No. 6 column ties

4 - No. 10 stub-column rein.

7 - No. 10 comp. rein. in each direction

250 mm

5 - No. 10 single bending shear reinforcement in each direction at centre of the slab

12 - No. 15 ten. rein. with 166 mm c/c in each direc.

150 mm

150 mm

1830 mm

1950 mm
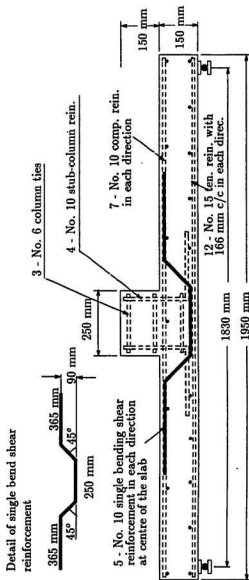
Figure 4.3: Dimension and reinforcement details of the slab with single bend shear reinforcement (HS18)
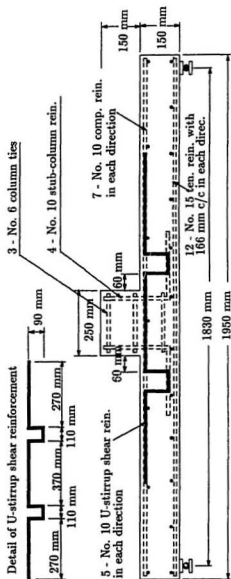
Figure 4.4: Dimension and reinforcement details of the slab with U-stirrup shear reinforcement (HS20)

Detail of U-stirrup shear reinforcement

270 mm | 170 mm | 270 mm
110 mm | 170 mm | 110 mm

5 - No. 10 U-stirrup shear rein. in each direction

90 mm

250 mm

60 mm

60 mm

3 - No. 6 column ties

4 - No. 10 stub-column rein.

7 - No. 10 comp. rein. in each direction

12 - No. 15 ten. rein. with 166 mm c/c in each direc.

150 mm

150 mm

1830 mm

1950 mm

60

Detail of double bend shear
reinforcement

Figure 4.5: Dimension and reinforcement details of the slab
with double bend shear reinforcement (HS21)

Details of shear-stud reinforcement (Studrail)

Anchor head (10 times cross section area of stud)

15 mm stud diameter welded

110 mm

Stud

Stud strip

270 mm

90 mm   60 mm   30 mm

36 - 15 mm diameter shear-studs

3 - 6 M column ties

4 - 10 M stub-column rein.

7 - 10 M comp. rein. in each direction

850 mm

150 mm

250 mm

90 mm 90 mm

60 mm

90 mm

12 - 15 M ten. rein. with 166 mm c/c in each direction

1830 mm

1950 mm

Figure 4.6: Dimension and reinforcement details of the slab with shear-stud reinforcement (HS22)
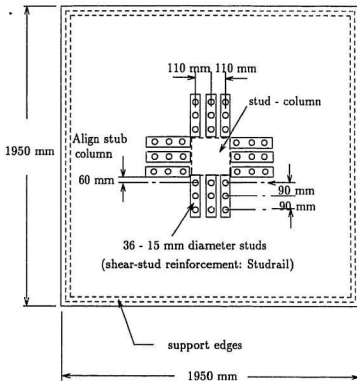
Figure 4.7: Arrangement of shear-stud reinforcement (Studrail) in Slab HS22
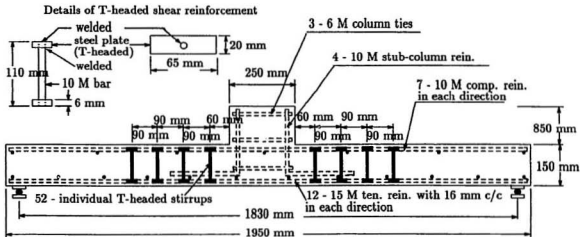
Figure 4.8: Dimension and reinforcement details of the slab
with T-headed shear reinforcement (HS23)
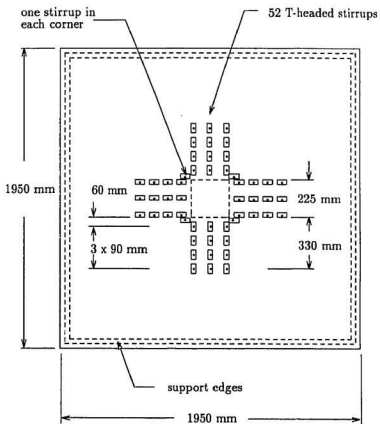
Figure 4.9: Arrangement of T-headed shear
reinforcement in Slab HS23

Table 4.1: Details of the test slabs in Series I and II

Specimens	Series	shear reinforcement	f_c' MPa	Bar size	c/c mm	h mm	d mm	ρ %
HS17	I	—	67	No. 15	166	150	120	1.093
HS19	I	—	61	No. 20	266	150	120	1.093
HS18	II	single-bend	68	No. 15	166	150	120	1.093
HS20	II	U-stirrups	74	No. 15	166	150	120	1.093
HS21	II	double-bend	72	No. 15	166	150	120	1.093
HS22	II	shear-stud	60	No. 15	166	150	120	1.093
HS23	II	T-headed	60	No. 15	166	150	120	1.093

reinforcement, while Slab HS21 had 10 mm double bend shear reinforcement. The U-stirrup and double bend shear reinforcement were arranged the same way as single bend shear reinforcement. The shear-stud reinforcement consisted of vertical steel rods (studs), a bottom anchor strip and the top anchor plates. as shown in Figs. 4.6 and 4.7. The bottom anchor strip is for holding the studs in their appropriate positions with the forms for case in construction. The top anchors is in the form of circular or square plates, the areas of which are at least 10 times the area of the stem (Elgabry and Ghali, 1990). The diameter of shear-stud reinforcement employed in this research program was 15 mm in diameter. A total of 36 studs were placed in Slab HS22. The T-headed shear reinforcement consisted of a 10 mm bar as a stem, two 25 × 65 mm steel plates individually welded on both sides as anchor plates. A total of 52 T-headed studs were placed in Slab HS23. Figs 4.10 and 4.11 show photographs of T-headed and shear-stud reinforcement arranged in Slab HS22 and HS23 in details, respectively.

4.3 Test set-up

Fig 4.12 shows a photograph of the test set-up. The loading frame was composed of four vertical wide flange steel columns connected by two horizontal cross wide flange steel beams braced by two channels as a K-shape brace construction. The frame was bolted to the floor using eight 40 mm anchor bolts spaced at 600 mm apart and four 38 mm based plates. The structural floor at M.U.N. structural laboratory is one meter thick heavily reinforced concrete floor. The test slab was mounted vertically on the inner face of rear side on the loading frame. The external loads were applied to the test slabs through a hydraulic actuator controlled by MTS machine and supported

Figure 4.10: Shear-stud reinforcement (Studrail) in construction (Slab HS22)
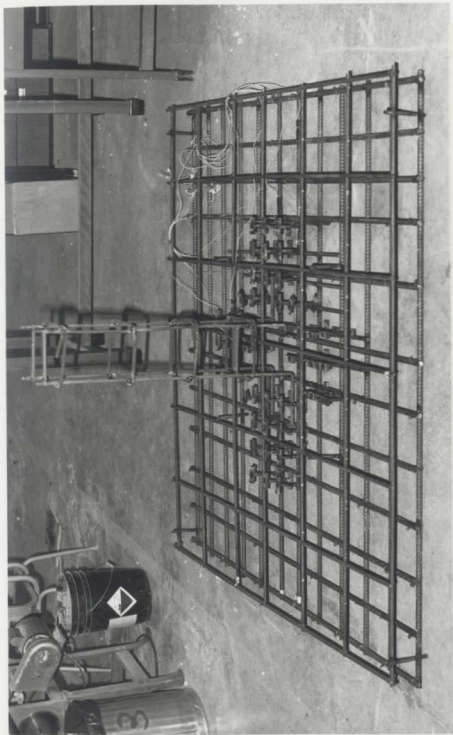
Figure 4.11: T-headed shear reinforcement in construction (Slab HS23)

on the inner face of the front side.

The slab was supported along the edge on a round steel bar welded to a steel plate fixed to the loading frame in order to simulate a roller support. Rubber packing pieces were provided immediately under the slab surface to insure uniform contact along the supports.

4.4 Instrumentation and measurements

4.4.1 Loading system

The load was applied to the test specimen through a hydraulic actuator using an MTS 850 structure test system. The actuator had a piston area of 324 cm^2 with a full stroke of 150 mm and a maximum capacity of 670 kN.

A closed loop system operating in a displacement control model was used for testing all of the seven slabs. The control system consisted of an MTS 410 Digital Function Generator, MTS 413 Master Control Panel, MTS 417 Counter Panel and MTS 430 Digital Indicator. Generally, structural testing can be performed with three modes of testing, namely, load control, stroke control and strain control. The stroke control testing technique was utilized throughout the tests in order to determine the descending branch of the load-deflection curve. The command signal was applied automatically by the control system with 15 mm per volt, while the feedback signal was provided by means of an built-in LVDT.

4.4.2 Deflections

The deflection of the slabs during loading was measured by a DC linear variable differential transformer (LVDT) which had a linearity of 0.3 % at 10 volts and sensitivity

Figure 4.12: Test set-up

of 16.92 mv/v.mm. Deflections were measured at two locations, namely at the centre of the slab and midway from the support line to the centre of the slab. The readings were obtained using a data acquisition system (Sciemetric-system 200) with 32 channels, in which there is one channel connected to the built-in LVDT. Thereafter, the voltage readings were converted to displacements using the LVDT calibration factor. Furthermore, the load-deflection curves were automatically plotted, using a x-y Hewlett Packard plotter connected to the MTS machine.

The displacement at the plate corners and at the mid-side of the top surface at the support lines were also monitored, using dial gauges with a one-hundredth of a millimetre precision.

4.4.3   Steel strains

The steel strains were measured in each connection at different locations by means of electrical strain gauges. Fig 4.13 shows a typical arrangement of the steel strain gauges. The strain gauges were 10 mm long, with a resistance of 120 Ω and a gauge factor of 2.04 $\pm$0.5 %. For protection against any possible water damage during casting, the strain gauges were coated with a protective sealant and then covered with a shrink tube waxed at the ends.

4.4.4   Concrete strains

The concrete strains were measured at different locations on the tension and compression faces of the concrete slabs by means of electrical strain gauges. Fig 4.14 shows a typical arrangement of the concrete strain gauges attached to compression face of the slabs. The concrete strain gauges were 50 mm long, with a resistance of 120 Ω and a gauge factor of 2.07 $\pm$ 0.5 %.
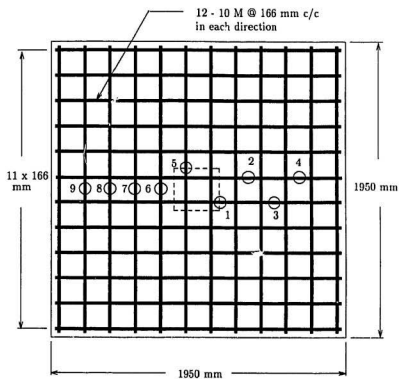
Figure 4.13: Steel strain gauge locations

A very thin layer of epoxy bonding agent was used to prepare a flat smooth surface on the concrete, to which the strain gauges were glued. The gauges were connected to a data acquisition system (Sciemetric-system 200).

4.5 Preparation of test slabs

4.5.1 Fabrication of the model

Concrete

The concrete mix proportions developed at M.U.N. engineering lab in a previous research program (Marzouk and Hussein, 1989) are given in Table 3.3 in Chapter 3. A 12 % replacement of cement by Type F fly ash and 8 % replacement by silica fume were used on basis of weight for all the test slabs. A superplasticizer of naphthalene formaldehyde bases, a neutralized vinso! air-entraining agent, and a retarder of non chloride base were employed in all mixes. The target strength was 70 MPa after 28 days. A total of six batches, 0.1 m^3 each, were used in casting each slab.

Reinforcing Steel

The reinforcing bars were cold-worked ribbed bars, CSA Grade 400, with a minimum characteristic strength of 400 N/mm^2. The actual characteristic strength was 490 N/mm^2, with an average ultimate tensile strength of 690 N/mm^2.

Formwork

The formwork which was used for casting all the slabs is shown in Fig 4.10. It consisted of a 2000 × 2000 mm plywood, while the sides of the form were made with 20 mm plywood. The formwork was constructed such that it can be dismantled
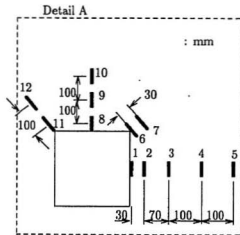
Figure 4.14: Concrete strain gauge locations

and re-used. The steel was tied together into a sturdy mat and lifted into the form. The reinforcing mat rested upon 20 mm wooden chairs. The chairs were placed far away from the punching zone in order to eliminate their effect on the observed shear strength. However, during casting great care was taken to insure that the cover provided was uniform.

4.5.2 Casting and curing

The mixing procedure developed at M.U.N. lab for high-strength concrete (Marzouk and Hussein, 1989) was adopted. Each concrete batch was poured into the mould and then vibrated using an electrical rod vibrator. When all the batches were cast, the vibrator was applied to the whole slab to insure its consistency. When full compaction was attained, the top face of the slab was then levelled and finished with a steel trowel. For determining the concrete compressive strength, three 150×300 mm (6×12 in) cylinders were taken from each batch in conjunction with casting of the principal test specimens.

After casting, the slab and its control specimens were covered with polythene sheeting. The formwork for the slab and the stub column was stripped 48 hours after casting; at the same time the cylinders were demoulded and transferred to a water tank for curing. The slabs were cured for two weeks by pouring water to its surface every 12 hours.

4.6 Test procedure

As mentioned before, the tests were carried out using a 670 kN capacity hydraulic actuator provided with displacement control. The test was conducted in a displace-

ment control mode of 8 mm per an hour increments. During the testing, the slabs were carefully inspected and the cracks were observed periodically. Also, the vertical deflection at the center of the slab, corner uplift, concrete strain gauge readings and steel strain gauge readings were recorded periodically.

Chapter 5

Test Results and Observations

5.1 Introduction

The results and observations obtained from testing seven high-strength concrete slabs with different types of shear reinforcement are given in this chapter. In particular, various measurements obtained from the experimental investigation (as described in chapter 4) are presented in the following sections. In addition, the crack patterns at failure are depicted by means of photographs. Due to the large amount of experimental data, only a few representative results are used in the presentation of variation of deflections, strains, etc.

As described in chapter 4, the slabs in Series I were used as reference specimens with no shear reinforcement. The slabs in Series II have five types of different shear reinforcement in order to examine the effect of shear enhancement on punching-shear behaviours.

5.2 Load-deflection characteristics

The load versus the deflection was applied through the stub column at the centre of each slab as described in Chapter 4. The load-deflection curves were obtained

from the LVDT readings connected to MTS machine, scanned constantly by a data acquisition system (Sciemetric-system 200), and displayed by a computer. The first yielding of the bottom reinforcement is indicated by a circle on each curve. Fig. 5.1 shows the load-deflection curves for slabs in Series I. Figs. 5.2 to 5.6 show the comparison of individual load-deflection curve in Series II with the curves in Series I. Table 5.1 gives the summary of measured deflections at the first yield of flexural (tension) reinforcement, ultimate loading capacity, as well as post-ultimate loading capacity (referred to as ultimate deflection) for all slabs. The comparison of the load-deflection characteristics of the individual slab in Series II with the corresponding mean value of the two reference slabs in Series I is discussed below.

The inclusion of different types of shear reinforcement except for the U-stirrup type improved the ultimate loading capacity as compared to the mean ultimate loading capacity of slabs in Series I (without shear reinforcement). Provision of shear enhancement also provided a post-ultimate behaviour when the ultimate loading capacity was reached, and can eliminate the so-called punching shear failure in three specific cases as it will be described in Section 5.4. However, the punching failure occurred and no post-ultimate loading capacity was observed for both of the reference specimens in Series I.

Slab HS18 (single bend shear reinforcement) only had a slight increase of 5 percent in ultimate loading capacity. In spite of this small contribution, it showed the best post-ultimate loading behaviour. The slab had a considerable ultimate deflection (the deflection at the post-ultimate loading capacity) with an associated loading capacity reaching 78 percent of its ultimate load; at the same time most of tension reinforcement yielded. Slab HS18 had an increase in ultimate deflection up to 71

Figure 5.1: Load-deflection characteristics at the centre of the reference slabs without shear reinforcement (Series I)
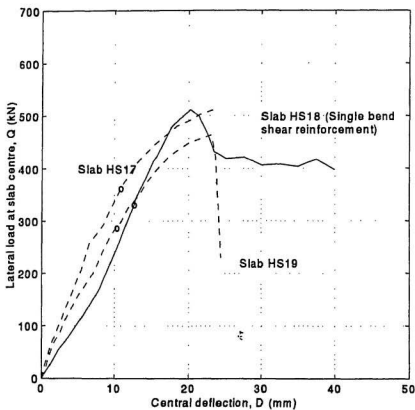
Figure 5.2: Load-deflection characteristics at the centre of the slab with single bend shear reinforcement (Slab HS18 in Series II)
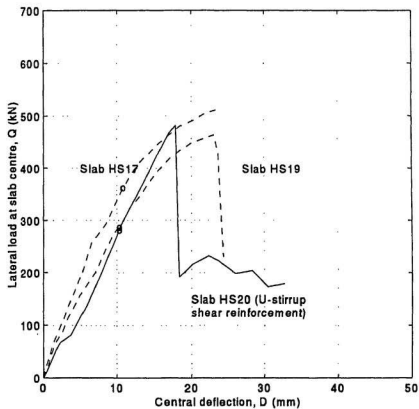
Figure 5.3: Load-deflection characteristics at the centre of the slab with U-stirrup shear reinforcement (Slab HS20 in Series II)
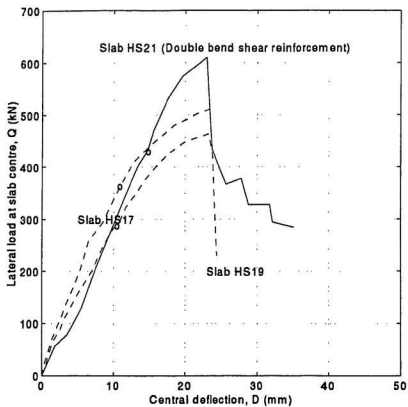
Figure 5.4: Load-deflection characteristics at the centre of slab with double bend shear reinforcement (Slab HS21 in Series II)
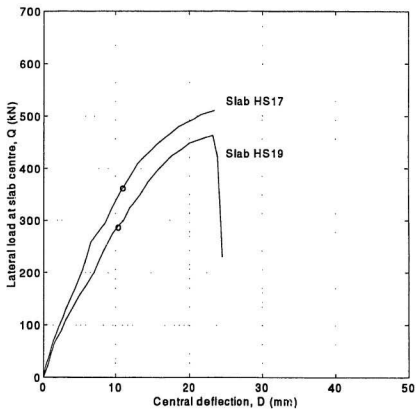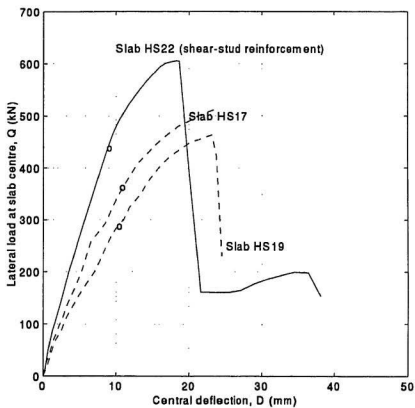
Figure 5.5: Load-deflection characteristics at the centre of slab with shear-stud reinforcement (Slab HS22 in Series II)
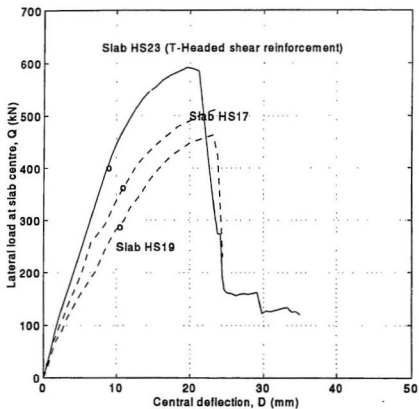
Figure 5.6: Load-deflection characteristics at the centre of slab with T-headed shear reinforcement (Slab HS23 in Series II)

Table 5.1: Deflection characteristics of test slabs

Specimens	Shear reinforcement	Series	f'_c MPa	First yielding ϵ_y $\mu\epsilon$x10^3	First yielding Q_y kN	First yielding Δ_y mm	Ultimate capacity Q_u kN	Ultimate capacity Δ_{Qu} mm	Post-ultimate capacity $Q_{\Delta u}$ kN	Post-ultimate capacity Δ_u mm
HS17	—	I	67	2.50	364.4	11.0	511.1	23.4	511.1	23.4
HS19	—	I	61	2.50	289.3	10.4	463.3	23.2	229.9	23.2
HS18	single-bend	II	68	2.50	333.8	12.7	511.7	20.2	396.8	39.8
HS20	U-stirrups	II	74	2.50	283.4	10.2	481.8	18.2	179.1	32.7
HS21	double-bend	II	72	2.50	431.4	14.8	609.7	22.9	284.1	35.1
HS22	shear-stud	II	60	2.50	440.3	9.1	605.1	18.3	153.3	38.7
HS23	T-headed	II	60	2.50	402.5	8.9	590.1	19.6	120.1	35.0

percent as compared to the corresponding mean value in Series I. However, there was no evidence of increase in ultimate loading capacity for Slab HS20 (U-stirrup shear reinforcement). It was observed that the loading capacity of Slab HS20 was the lowest among Series II. The post-ultimate loading capacity dropped to 37 percent of its ultimate load after punching occurred. The ultimate deflection was increased by 40 percent. In the case of Slab HS21 (double bend shear reinforcement), an increase in the ultimate loading capacity up to 25 percent was reached. The post-peak loading capacity, subsequently after reaching the ultimate loading capacity, dropped to 74 percent of the ultimate value, and then gradually reduced to 47 percent at the final failure. The slab had an increase of 51 percent in ultimate deflection. In the case of Slab HS22 (shear-stud reinforcement), an increase of 24 percent in the ultimate loading capacity was reached. The loading capacity suddenly dropped to 30 percent of its ultimate load at the beginning of the post-peak loading period. Then the post-peak loading capacity gradually reached to 35 percent of the ultimate load until the ultimate deflection of 35 mm. The increase in ultimate deflection was up to 66 percent. In the case of Slab HS23 (T-headed shear reinforcement), the overall behaviour in the load-deflection curve was practically identical to Slab HS22. An increase in the ultimate loading capacity of 21 percent was reached. However, the post-peak loading capacity of Slab HS23 dropped in a similar fashion to Slab HS19 as shown in Fig. 5.4. An increase of 50 percent in ultimate deflection was also reached over the reference specimen.

It should be noted that the latter three types of shear reinforcement (the double bend, shear-stud, and T-headed shear reinforcement) have almost the same contribution to improving the ultimate loading capacity. In all three cases, their ultimate

loading capacity as well as ultimate deflection were practically identical. The ultimate loading capacity of these slabs is finally governed by the flexural reinforcement ratio, since the punching shear capacity is enhanced enough to prevent punching shear failure. The flexural reinforcement ratio of 1.093 percent was designed for all slabs. A greater increase in the ultimate loading capacity could be expected in the slabs including these three types of shear reinforcement, if a higher flexural reinforcement ratio was specified. The double bend, shear-stud and T-headed shear reinforcement are effective types of shear reinforcement for enhancing the punching shear capacity.

5.3   Ductility and energy absorption

Ductility U is defined as the ratio of the ultimate deflection Δ_u to deflection at first yield Δ_y. The energy-absorption capacity is defined as the area under the load-deflection curve. The ductility at failure and the energy-absorption capacity of all tested slabs, as defined above, are given in Table 5.2.

The contribution to both ductility and energy absorption by different types of shear reinforcement was obtained from test observation, while compared to the reference slabs. The mean value of ductility of slabs in Series II reached an increase of 55 percent while compared to the corresponding value of slabs in Series I. Slab HS21 (double bend shear reinforcement) had no increase in ductility, because its first yielding deflection was relatively larger. Therefore, the ratio of its ultimate deflection to the first yielding deflection was not improved. The increase in ductility U for slabs in Series II ranged from 43 to 95 percent compared to the mean value of ductility U in Series I, except for the case of Slab HS21.

Corresponding to the increase in ductility U, the energy absorptions of slabs in

Table 5.2: Observed ductility and energy absorption

Specimens	Shear reinforcement	Series	f_c' MPa	Steel ratio ρ (%)	Ductility U Δ_u/Δ_y	Energy absorption kNmm10^3
HS17	—	I	67	1.0	2.13	7.92
HS19	—	I	61	1.0	2.24	7.03
HS18	single-bend	II	68	1.0	3.14	13.56
HS20	U-stirrups	II	74	1.0	3.22	7.89
HS21	double-bend	II	72	1.0	2.37	11.97
HS22	shear-stud	II	60	1.0	4.27	12.50
HS23	T-headed	II	60	1.0	3.93	12.14

Series II also increased. In terms of the mean value, the energy absorption of Series II was 55 percent higher than that of Series I. Slab HS18 (single bend shear reinforcement) showed the largest energy absorption among all slabs in Series II (with different types of shear reinforcement). The energy absorption value of Slab HS18 was almost double the mean value of Series I. However, slab HS20 (U-stirrup) had no increase in energy absorption. It is confirmed that the U-stirrups behaved inefficiently with regard to the punching shear capacity. Seible (1980) reported such behaviour and indicated that unless the U-stirrups enclosed the top and bottom flexure reinforcement of the slab and were welded as a wire fabric cage, it will not become an effective shear reinforcement. This greatly complicates the placement of flexure reinforcement, and become impossible in practical construction.

5.4   Cracking and failure pattern

All slabs in Series I and II were designed to yield a ductile shear failure as detailed by Marzouk and Hussein (1991). The ductile shear failure mode can be characterized by yielding of the tension steel in a certain area around the column stub before punching occurs. From the test observation, flexural cracking occurred first in all slabs, and it advanced roughly from the column outlines towards the slab edges parallel to flexural (tension) reinforcement. Subsequently, tangential cracks developed around the vicinity of the column outline. Failure patterns of the tested slabs in Series I and II are shown in Figs. 5.7 to 5.13.

In terms of inclined cracking, the cracking development in the conical portion of Slab HS22 (shear-studs) and HS23 (T-headed stirrups) are carefully examined. Fig. 5.14 shows the part of the slab stub column, which was carefully taken out from the
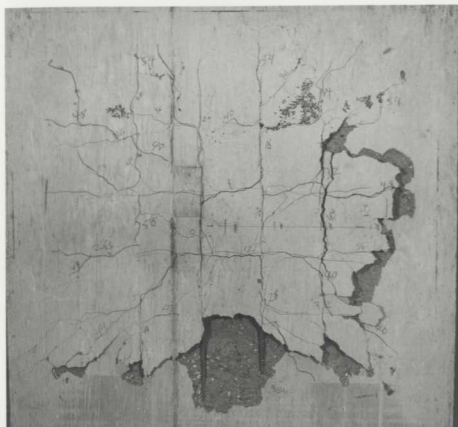
Figure 5.7: The failure pattern of Slab HS17 without shear reinforcement in Series I

Figure 5.8: The failure pattern of Slab HS19 without shear reinforcement in Series I

Figure 5.9: The failure pattern of Slab HS18 (single bend shear reinforcement) in Series II
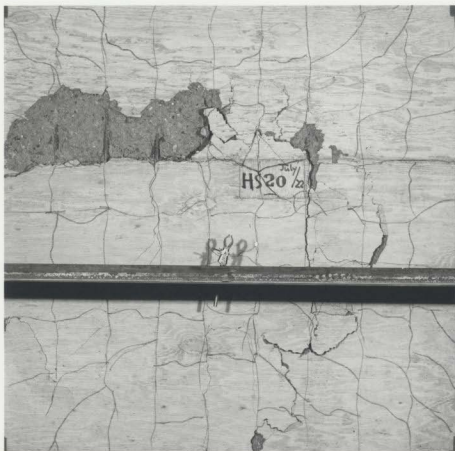
Figure 5.10: The failure pattern of Slab HS20 (U-stirrup shear reinforcement) in Series II
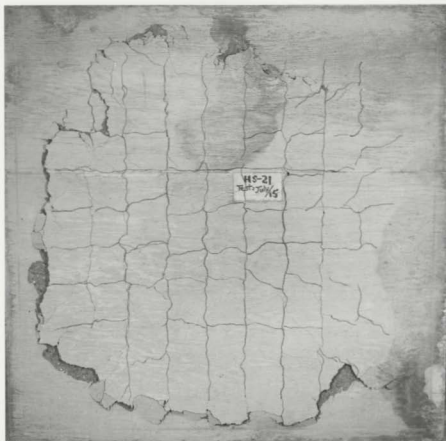
Figure 5.11: The failure pattern of Slab HS21 (double bend shear reinforcement) in Series II
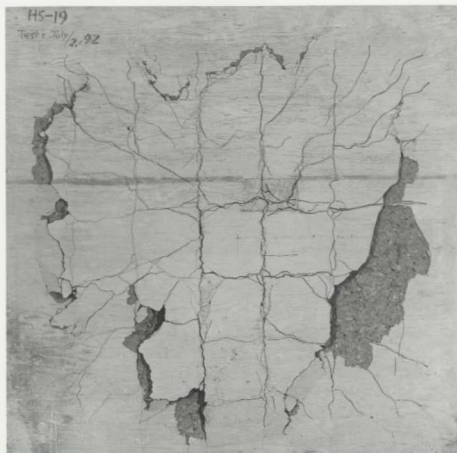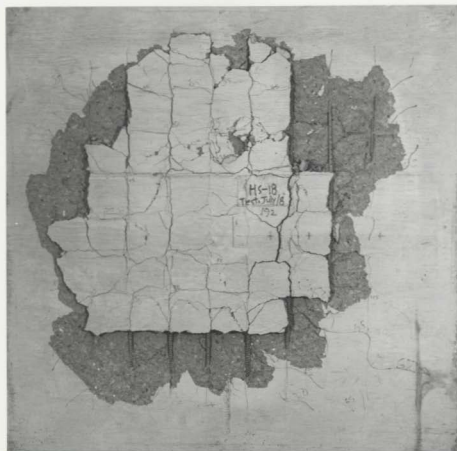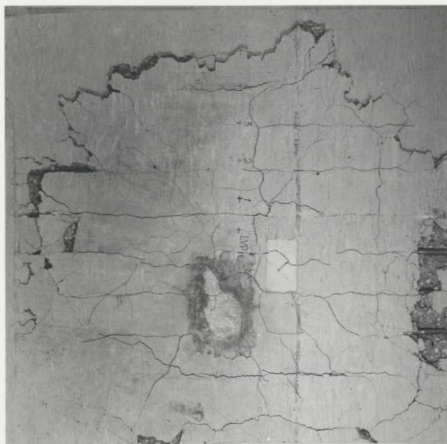
Figure 5.12: The failure pattern of Slab HS22 (shear-stud reinforcement) in Series II
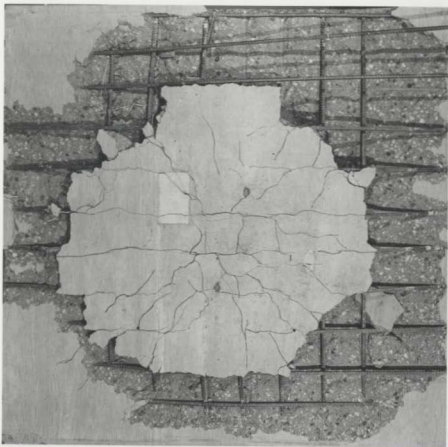
Figure 5.13: The failure pattern of Slab HS23 (T-headed shear reinforcement) in Series II

failure slab, HS23. Extensive inclined shear cracks were observed in the connection zone beyond a distance 1.0 d to the column face. These cracks surfaced with a small slope under concrete cover at the top side of the slab. They extended to the last vertical shear stirrup rows far to four column faces, and then penetrated into the slab with a slope of 45 degrees. Neither the shear-studs, nor the T-headed stirrups were intersected by the inclined shear cracks. The final failure progressed with the most of bottom bars were pulled out. Slabs were divided into two parts along the horizontal split crack at the top and the inclined cracks with a slope of 45 degree. At the conclusion of the tests, quite larger areas enveloped by out-most tangential cracks were observed on the bottom face of the slabs provided by double bend, shear-stud and T-headed shear reinforcement. In these three cases, the punching shear failure was eliminated, and finally transformed into a flexural failure.

5.5 Strain distribution

In order to determine the strain distribution in flexure reinforcement, the strain measurements were made for all test slabs as arranged in Fig. 4.13. The yield strain of a steel bar reached 2500 microstrains according to the experimentally obtained stress-strain curve of the steel reinforcement. The flexural reinforcement yielded at the column edge before punching took place in the reference slabs without shear reinforcement in Series I. For the slab with double bend, stud and T-headed shear reinforcement, the yielding advanced uniformly to a larger radius than that of the reference slabs. It is evident that the strain of the flexural reinforcement was inversely proportional to the radius for all test slabs, measured from the center of the slab to the point where strain is determined. The highest strain and consequently initial
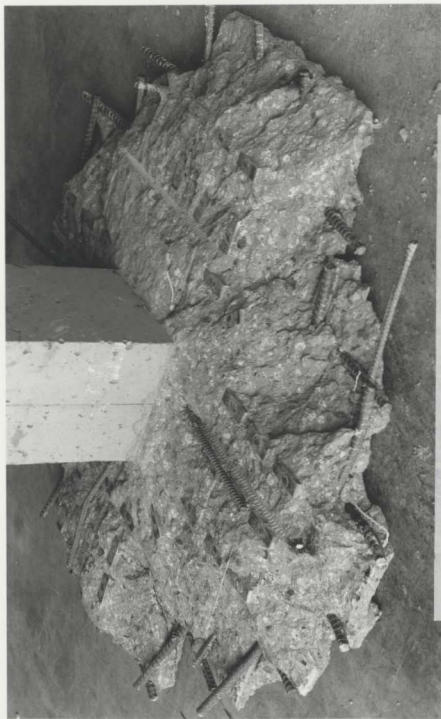
Figure 5.14: A typical punching shear core of test slab HS23 in Series II

yielding occurred below the stub-column.

In terms of strain distribution of different shear reinforcement, the strain was measured at the bent bar of the double bend shear reinforcement for Slab HS21, and at the stem of shear-stud and T-headed shear reinforcement for Slabs HS22 and HS23, respectively. Figs. 5.15 to 5.17 show a typical curve of load versus the strain of shear reinforcement for these three slabs.

The strain in the bent bar of the double bend shear reinforcement was close to yielding strain of 2000 microstrains at ultimate load for Slab HS21, as shown in Fig 5.15. Therefore, the double bend shear reinforcement was very effective in resisting the shear force. The strain level measured at the stem of studs (Slab HS22) near column faces, even at ultimate load, was relatively small (less then 400 microstrains) since the stud with a 15 mm diameter was specified. It should be noted that the total amount of shear-stud reinforcement designed in Slab HS22 was approximately equal to the amount T-headed shear reinforcement (in weight) in Slab HS23. The strain of the T-headed shear reinforcement at the same location was much higher, and reached a value of 1500 microstrains at ultimate load. The strain at this location developed very fast when the load level reached 80 percent of its ultimate load, as shown in Fig 5.17. These three types of shear reinforcement prevented the shear cracking development. The punching shear failure was finally eliminated. Their ultimate failure was flexurally controlled.

Measurements were made to determine the distribution of the concrete strain in both tangential and radial directions around the stub column of the slab, as shown in Fig. 4.14 in chapter 4. The tangential strains were high at the column face, but decreased rapidly as the radius increased. The strains on the tangential direction
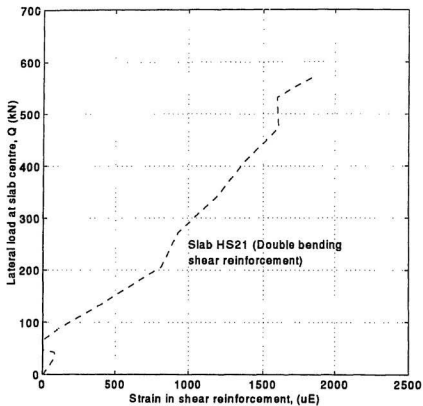
Figure 5.15: Typical load versus the strain in double bend shear reinforcement of Slab HS21
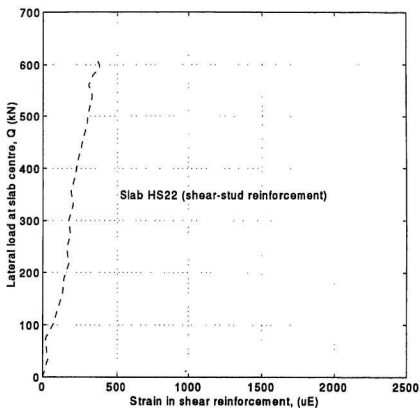
Figure 5.16: Typical load versus the strain in shear-stud reinforcement of Slab HS22
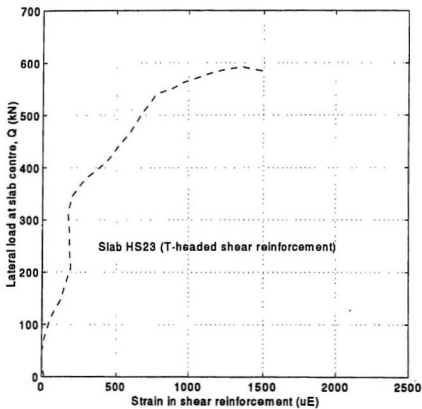
Figure 5.17: Typical load versus the strain in T-headed shear reinforcement of Slab HS23

through the corners of the column stub (Gauge 4, Fig. 4.14) were higher than those at the middle of the column face (Gauge 1, Fig. 4.14). In all these cases, they reached a compressive value of 0.003 in loading step prior to failure. This indicates a concentration of stress at the corner of the column stub (Marzouk and Hussein, 1991). Fig. 5.18 shows a typical load versus concrete strain curve measured at these positions. Neither the concrete strains in the tangential nor the radial directions reached a limiting value of 0.0035 for any of the tested slabs.
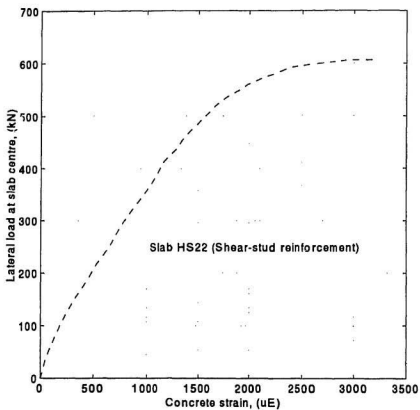
Figure 5.18: Typical load versus concrete strain near the mid of the column face of Slab HS22

Chapter 6

Finite Element Analysis of Test Slabs

6.1 Introduction

A non-linear finite element (F. E.) analysis was carried out on the test slabs as an analytical investigation. A new F. E. model implementing a three-dimensional element was developed in this study for the necessity of incorporating any types of out-of-plane shear reinforcement. Three-dimensional twenty node brick element and plasticity-based concrete model were implemented in a general purpose F. E. code, ABAQUS (Hibbitt et al, 1993), to perform F. E. analysis on the five slabs with different types of shear reinforcement in Series II. A simpler two-dimensional F. E. model with eight node thick shell element developed in a previous research program (Marzouk and Chen, 1993) was adopted to perform F. E. analysis on the two reference slabs in Series I, since it can perform satisfactorily F. E. analysis with economic CPU time consuming on the high-strength concrete slabs with no shear reinforcement. The comparison on the predicted-to-measured results was addressed in terms of ultimate load and its associated deflection as well as punching shear distribution.

6.2 Finite element program

In this study, one half of a slab with different types of shear reinforcement in Series II was modeled with 3×6 mesh using three-dimensional brick elements with twenty nodes with three displacement degrees of freedom per node. Totally, 18 elements were used. The finite element mesh and the three-dimensional brick element employed are shown in Fig. 6.1. A reduced 2×2×2 Gaussian integration rule over the element faces was adopted. Boundary conditions were symmetrical on one edge of the mesh. Special nonlinear spring element with no tension stiffness and reaching infinite values in compressive stiffness was applied along the edges of the mesh in order to simulate the actual test specimens. The test slabs were simply supported along all four edges with corners free to lift, as described in chapter 4.

Reinforcement is treated as a one-dimensional strain element (Hibbitt et al, 1993) that can be defined singly or embedded in any orient surfaces. The reinforcing bar is then superimposed on mesh of standard element types used to model plain concrete. The inclined types of shear reinforcement in Slab HS18 (single bend) and HS20 (double bend) were represented simply by a uniform thickness layer inside the element inclined at 45 degree. The vertical types of U-stirrup, shear-stud and T-headed shear reinforcement were depicted individually inside the three-dimensional brick element. The location of each vertical rebar was determined by choosing one of three isoparametric directions in the three-dimensional element and two fractional distances across an element face that is orthogonal to the chosen isoparametric direction. Each isoparametric direction is orthogonal to one of the three orthogonal faces defined in the element. Cross-sectional area of each rebar was described.

The realistic material properties of high-strength concrete from our laboratory
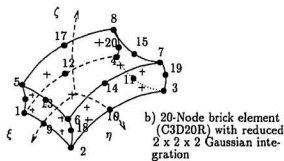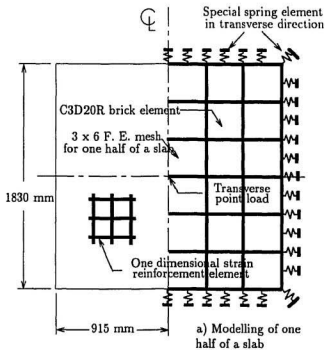
Figure 6.1: Geometric mesh with three-dimensional brick element for slabs in Series II

testing was incorporated into an incremental elastic-plastic concrete model. The complete uniaxial compressive stress-strain relation was recorded with the secant modulus of elasticity of 35 GPa at 0.4 f'_c, including a concrete compression softening region. A standard plasticity approach was used to describe the behaviour of reinforcing bar material. The stress-strain curves for 10 mm and 15 mm diameter (CSA Grade 400) were also measured in the laboratory.

As reviewed in chapter 2, the results from the non-linear F. E. analysis for reinforced concrete structures are largely dependent on the stress-strain relationships, failure criteria used, simulation of steel reinforcement, and interaction between the steel and concrete. Proper modeling of cracking and post-cracking behaviour of reinforced concrete is especially crucial. The concrete model is based on the classical concepts of plasticity theory: a strain rate decomposing into elastic and inelastic strain rates; elasticity; yield; flow; and hardening, which allows for strain softening after both cracking and crushing. The smeared crack method based on the concept of stress discontinuity while maintaining displacement continuity was used in this investigation. Cracking is assumed to occur when the stress reaches a failure surface according to the coulomb line failure criteria. Cracking is irrecoverable and remains throughout the rest of calculation. The concrete behaviour is considered independently of the reinforcement steel. Once concrete has cracked, effects associated with the reinforcement steel/concrete interface including bond slip, dowel action and tension stiffening are modeled by losing concrete strength through a softening mechanism. The strain softening after cracking reduces the stress linearly to zero in the concrete modeling to simulate load transfer across cracks through the reinforcement steel. The interaction between reinforcement and concrete are represented through

the parameter of "Tension Stiffening". The finite element program is fairly sensitive to the tension stiffening values for each particular practical case.

The modified Riks algorithm (Hibbitt et al, 1993) was selected to obtain effectively the static equilibrium solution for unstable response in this F. E. model. A proportional loading history was employed with this approach.

For the slabs used in Series I as reference specimens (without shear reinforcement), a much simpler F. E. model developed in a previous research program as mentioned above was used to perform the analysis. The plasticity-based material model described above was incorporated in this F. E. model. One quarter of the slab was modeled with $3 \times 3 \times 3$ mesh using eight node thick shell element. A 2×2 Gaussian integration was adopted over the plane of each element, while a nine point Simpson rule was used over the mesh. Totally, 9 elements were used. Boundary condition was symmetrical on two edges of the mesh, and the same spring element was applied on other two edges of the mesh. The geometric mesh and the eight-node quadrilateral shear-flexible shell element are shown in Fig. 6.2. Flexural reinforcement was represented simply by four layers of uniform thickness located at a constant relative depth inside the thick shell element.

6.3 Comparison of finite element analysis to test result

The F. E. analysis was conducted on the comparison of predicted-to-measured ultimate loads and the associated deflections at the center of the test slabs. The distribution of transverse shear stress under the ultimate load, referred to as punching shear, was also discussed based on the numerical approach in the next section. As

a) Modelling of one quarter of a slab

b) 8-Node quadrilateral thick shell element (S8R) with 2x 2 Gaussian integration
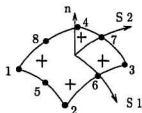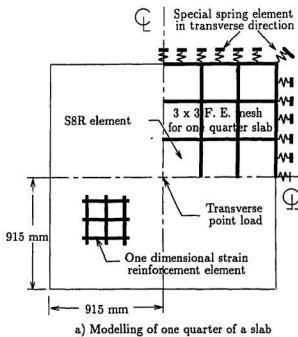
Figure 6.2: Geometric mesh with thick shell element for slabs in Series I

described in the previous section, the three-dimensional model was employed in the prediction of slabs with different types of shear reinforcement in Series II, and a simpler two-dimensional model was adopted to conduct the numerical approach for the reference slabs without shear reinforcement in Series I. Table 6.1 shows a detail of the comparison of predicted-to-measured ultimate loads and the associated deflections at the center of these test slabs.

The analytical investigation indicated that the two-dimensional finite element model with eight node thick shell elements performed satisfactorily for slabs in Series I. The ratios of predicted-to-measured ultimate loads were 0.98 and 1.05 for Slab HS17 and HS19 respectively, while the ratios of the associated central deflections were 0.96 for the both slabs. However, the agreement between the prediction of this numerical model and the test results for the slabs in Series II was less accurate. It was observed that all ultimate loads computed by the two-dimensional model were lower than those measured from test results. This behaviour can be explained due to the absence of implementing shear reinforcement in the model. As described before, it is impossible to model any types of vertical and/or inclined shear reinforcements in a two-dimensional finite element model using shell elements. With the application of a three-dimensional brick element, there was a reasonable agreement between the predictions by the F. E. model and the measurement by the tests in slabs in Series II. The ratios of predicted-to-measured ultimate loads ranged from 1.07 to 1.31 with an average value of 1.18 and a standard deviation of 0.10. The ratios of the associated deflections at the center of the slabs ranged from 0.83 to 1.01, while the average value was 0.91 with a standard deviation of 0.06.

Table 6.1: Comparison of F. E. analyses to the test results in ultimate loading capacity and its associated deflection

Specimens	Series	Shear reinforcement	f_c' MPa	Bar size	Test result Q_u kN	Test result Δ_{Q_u} mm	F. E. analysis Q_u kN	F. E. analysis Δ_{Q_u} mm	F. E./Test Q_u	F. E./Test Δ_{Q_u}	Model*
HS17	I	—	67	No. 15	511.1	23.4	502.3	22.5	0.98	0.96	2-D
HS19	I	—	61	No. 20	463.3	23.2	484.4	22.2	1.05	0.96	2-D
HS18	II	single-bend	68	No. 15	511.7	20.2	660.1	18.0	1.29	0.89	3-D
HS20	II	U-stirrup	74	No. 15	481.8	18.2	632.4	18.3	1.31	1.01	3-D
HS21	II	double-bend	72	No. 15	609.7	22.9	690.4	18.9	1.13	0.83	3-D
HS22	II	shear-stud	60	No. 15	605.1	18.3	645.3	17.2	1.07	0.94	3-D
HS23	II	T-headed	60	No. 15	590.1	19.6	645.3	17.2	1.09	0.88	3-D

* 2-D: Two-dimensional finite element model; 3-D: Three-dimensional finite element model

6.4 Punching shear distribution

The investigation of transverse shear stress distribution under the ultimate load, referred to as punching shear, was carried out by using the F. E. analysis since it is difficult to measure this distribution and its associated value from the experimental investigation. Fig. 6.3 shows the punching shear distribution in the slabs with different types of shear reinforcement in Series II. Fig. 6.3 was interpreted from the diagrams of the transverse shear stress contours provided by the three-dimensional model. The punching shear distribution was characterized by figuring out the contour enclosing the maximum shear value in the vicinity of the loading stud. A typical contour diagram provided by the slab (HS23) with T-headed shear reinforcement is presented in Fig. 6.4. The contour enclosing the maximum shear stress near the loading face is shown along one of two in-plane symmetrical axes in this figure.

As shown in Fig. 6.3, the punching shear distribution formed four identical concentrated fields. The center of these fields was located at a distance 1.5 d to the loading face. It should be mentioned that this center was distributed on the top side of the slab because the shear contours were provided by the three-dimensional model on the top face of the element. However, the punching shear distribution in the mid position of the section perpendicular to the plane of a slab is more interesting in practical design rules. The punching shear in this mid position could be expected at a distance 2.0 d to the loading face. This expectation is based on the following rational assumption. The inclined punching shear cracking should surfaced on the top side of the slab at a distance 1.5 d to the loading face, and then, are supposed to penetrate through the slab section with 45 degrees. Therefore, the inclined cracking will be located at a distance 2.0 d in the mid position of the slab section. When effective
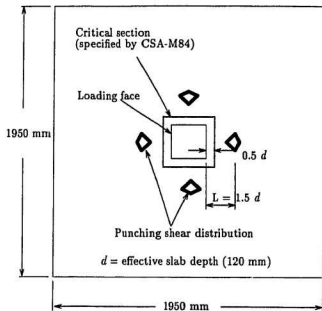
Figure 6.3: Punching shear distribution from three-dimensional model for slabs in Series II
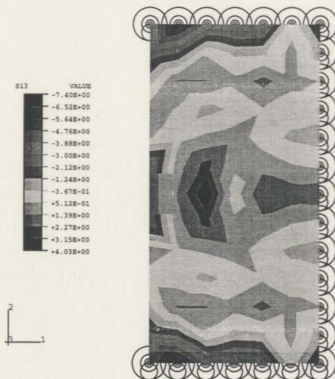
Figure 6.4: A typical diagram of the transverse shear stress contours provided by the three-dimensional model

shear reinforcement was provided, the inclined cracking is intercepted or prevented by the shear reinforcement, but the punching shear stress remains at the location. It should be highlighted that this punching shear distribution is far beyond the so-called critical section specified by CSA-A23.3-M84 (1984) code. According to the design code, the critical section for perimeter punching shear is located so that the perimeter is a minimum and must not be closer than 0.5 d to the loading stud face. This is rationally based on a simple linear assumption, and excludes the contribution of shear reinforcement to punching shear distribution. Hence, the shear resistance force of concrete, V_c, recommended by the design code is conservative for the slabs provided with effective shear reinforcement.

The numerical investigation revealed that the punching shear in the slabs provided with shear reinforcement was located out of a distance 0.5 d to the loading stud face. As described before in Chapter 5, the extensive inclined cracking surfaced at the top side of the slab at a distance of 1.0 d to 1.5 d from the column face. The test observation from the slabs with vertical types of shear reinforcement supports the provision by the F. E. analysis with the three-dimensional model.

Fig. 6.5 shows the punching shear distribution for the two reference slabs in Series I. The contours relative to punching shear were provided by the two-dimensional model. A typical contour diagram provided by a reference slab (HS17) is presented in Fig. 6.6. The contour enclosing the maximum shear stress is shown along one of two in-plane symmetrical axes in this figure. Similar to the provision by the three-dimensional model, the contours enclosing the maximum shear stress also formed four identical concentrated fields, but the center of these fields located at a distance 0.2 d from the loading face. The code specification of critical section, i. e. a distance 0.5 d,

is practically identical to the provision by two-dimension model in the slabs without shear reinforcement.

In terms of punching shear value, a comparison of the F. E. analysis with punching shear resistance is given in Table 6.2. τ_{max} is the maximum shear stress provided by shear stress contour diagrams as described above, v_r is unfactored shear resistance equal to $0.4\sqrt{f_c'}$ for the slab without shear reinforcement in Series I and $0.6\sqrt{f_c'}$ for the slab with different types of shear reinforcement in Series II, respectively. The ratio of predicted maximum shear stress to punching shear resistance, (τ_{max}/v_r), was 1.24 and 1.27, respectively for Slab HS17 and HS19 (two reference slab in Series I). The corresponding ratio for slabs with different types of shear reinforcement in Series II ranged from 0.72 to 0.93 with a mean value of 0.86 and a standard deviation of 0.08.

Based on the comparison and discussion above, a new plasticity-based concrete finite element model employing three-dimensional brick element with twenty nodes and a reduced 2×2×2 integration rule over the element faces is recommended for the finite element analysis of slabs with different types of shear reinforcement. The numerical investigation provided a reasonable agreement between the prediction and measured test results of ultimate load and its associated deflection, and revealed the punching shear distribution on the slabs placed shear enhancement. Currently, there is a growing evidence of emphasizing the development of three-dimensional constitutive models for concrete structures and the implementation of these models into finite element environment for non-linear analysis of reinforced concrete structures. The analytical work conducted in this thesis was an attempt in this field.
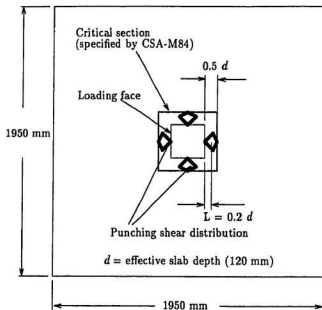
Figure 6.5: Punching shear distribution from ftwo-dimensional model for slabs in Series I

SECTION POINT 5

TSHR23   VALUE
-4.55E+00
-3.89E+00
-3.23E+00
-2.57E+00
-1.91E+00
-1.25E+00
-5.91E-01
+6.95E-02
+7.30E-01
+1.39E+00
+2.05E+00
+2.71E+00
+3.37E+00
+4.03E+00
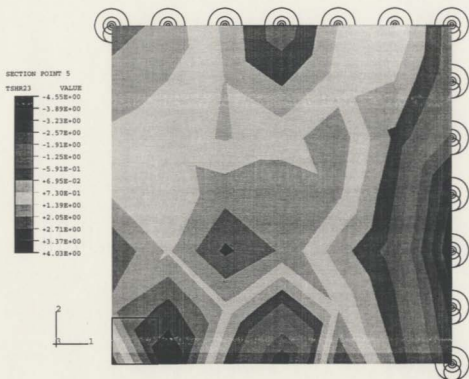
Figure 6.6: A typical transverse shear stress contour diagram provided by the two-dimensional model (the reference of HS17)

Table 6.2: Comparison of predicted maximum transverse shear stress to punching shear resistance

Specimens	Series	Shear reinforcement	f_c MPa	Shear capacity v_r MPa	F. E. analysis τ_{max} MPa	L^* d	Model	Ratio of τ_{max}/v_r %
HS17	I	—	67	3.27	4.04	0.2	2-D	1.24
HS19	I	—	61	3.12	3.95	0.2	2-D	1.27
HS18	II	single-bend	68	4.05	3.66	2.0	3-D	0.90
HS20	II	U-stirrups	74	5.16	3.72	2.0	3-D	0.72
HS21	II	double-bend	72	5.09	4.75	2.0	3-D	0.93
HS22 ·	II	shear-stud	60	4.65	4.03	2.0	3-D	0.87
HS23	II	T-headed	60	4.65	4.03	2.0	3-D	0.87

* L is a distance from the maximum shear stress to the loading face, and d is the effective depth of the slab

Chapter 7

Conclusions

The present research investigation was carried out in three stages, viz., material investigation, experimental tests on slabs and a numerical approach with finite element analysis to predict the punching shear capacity of the test slabs. The material part involved an experimental program carried out to study the effects of cold ocean environment under freeze-thaw cycles, simulated under laboratory conditions, on the high-strength tensile properties. The experimental testing program was conducted on seven high-strength concrete slabs with five different types of shear reinforcement. The study included structural behaviour of seven high-strength concrete slabs including five shear enhancement systems. In addition, a finite element analysis was performed on all the slabs to compare with the measured test results. A suitable F. E. model is recommended for slabs with different shear reinforcement. The following conclusions can be drawn from the present research:

7.1   Material investigation

The effects of freezing and thawing on the tension properties of air-entrained high-strength concrete were investigated. Two types of specimens were used in the in-

vestigation: standard (75×75×350 mm) concrete prisms and thin direct tension (20×75×300 mm) specimens. The specimens were exposed to 700 freeze-thaw cycles in accordance with ASTM C 666. At every 100 cycles of exposure, three standard prisms were tested for modulus of rupture and two direct tension specimens were tested for tensile strength. The same test procedure was repeated on normal strength concrete specimens to compare the durability of high-strength concrete to normal strength concrete. The conclusions of the investigation can be summarized as follows.

1. For the standard prisms (75×75×350 mm), the average value of the relative dynamic modulus of elasticity from resonant frequency tests after 300, 500 and 700 cycles was 88%, 85% and 83% for high-strength concrete and 73%, 61% and 45% for normal strength concrete, respectively. Therefore, the freeze-thaw durability of high-strength concrete is much higher than that of normal strength concrete.

2. The average modulus of rupture after 700 cycles of exposure was 85% and 40% of the original values for high-strength and normal strength concrete, respectively. The superior performance of high-strength concrete can be explained by the lower permeability and higher strength.

3. The average values of the relative dynamic modulus of elasticity for the direct tension (20×75×300 mm) specimens after 300, 600 and 700 cycles were 82%, 69% and 66% for high strength concrete and 72%, 54% and 39% for normal strength concrete, respectively. The greater deterioration compared with the standard prisms can be attribute to the smaller dimensions of the tension spec-

imens.

4. The direct tensile strength was found to be 4.2% and 3.4% of the compressive strength before cycling, at 0 and 700 cycles, respectively. The average value of cracking strain was found to be $65\mu\epsilon$ after 700 cycles of freezing and thawing compared with $115\mu\epsilon$ before the cycling.

5. The calculated value of fracture energy of high-strength concrete after 700 cycles was about 70% of the original value before cycling. Also, the area under the descending portion of the stress-strain curve after 700 cycles was about 3.5 times greater than the area under the ascending portion , compared to 5 times for the case before cycling.

7.2 Experimental investigation on test slabs

Tests were conducted on seven concrete slabs and five shear enhancement systems and the results were analyzed in detail. From the present investigation the following conclusions were reached:

1. Double bend, shear-stud and T-headed shear reinforcement are the most efficient shear enhancement for punching shear capacity of high-strength concrete plates.

2. An increase in ultimate loading capacity was provided by placing the efficient shear reinforcement. The ultimate loading capacity was increased by more than 20 percent for the above three types of shear reinforcement, while compared to the mean value of ultimate load for slabs without shear reinforcement.

3. Punching shear failure can be controlled by three effective types of shear reinforcement (double bend, shear-stud and T-headed shear reinforcement). Punching shear can be eliminated and transformed into flexural failure for the high-strength concrete plates utilizing the flexural reinforcement in a much better fashion.

4. The slab ductility and energy absorption were significantly increased by shear reinforcement as explained in this research program, except for the type of U-stirrup shear reinforcement which energy absorption value was relatively low.

5. U-stirrup is not an efficient type of shear reinforcement for the high-strength concrete plates. It did not provide any increase in ultimate loading capacity, and only had a slight contribution to energy absorption.

6. The use of high-strength concrete slabs provided with special shear reinforcement will solve all the durability, cracking and punching shear problems.

7.3   Numerical investigation

An analytical investigation was carried out on the test slabs using a non-linear finite element analysis. The comparison on the predicted-to-measured results has been presented and discussed in details. The significance and contribution of the present investigation was concluded as following:

1. A new finite element model implementing a three-dimensional element was developed in this study for the necessity of incorporating any types of out-of-plane shear reinforcement in order to predict the structural behaviours of the slabs with different types of shear reinforcement practicably.

2. A reasonable agreement between the prediction by the three-dimensional model and the experimental results has been obtained. The ratios of predicted-to-measured ultimate loads on five slabs with different types of shear reinforcement was found ranging from 1.07 to 1.31 with an average value of 1.18 and a standard deviation of 0.10. The ratios of the associated deflections at the center of these slabs ranged from 0.83 to 1.01, while the average value was 0.91 with a standard deviation of 0.06.

3. The finite element analysis is helpful for investigating the punching shear distribution since it is difficult to measure the transverse shear stress and its distribution in slabs from the test experiment. The prediction by the three-dimensional model reveals that the punching shear was located far beyond a distance 0.5 d to the loading face. The punching shear in the slabs provided with adequate shear reinforcement was located at the distance 1.5 d on the top side of the slabs and 2.0 d in the mid position of the section perpendicular to the plane of the slab. CSA-A23.3-M84 design code excludes the effect of shear reinforcement on determining the location of the so-called critical section. The shear resistance force of concrete, V_c, recommended by the code is conservative for the slabs with effective shear reinforcement.

4. A 20 node brick element can be recommended to model the slabs with different types of shear reinforcement. Currently, there is a growing evidence of emphasizing the development of three-dimensional constitutive models for concrete structures and the implementation of these models into finite element environment for non-linear analysis of reinforced concrete structures. The analytical work conducted in this thesis was an attempt in this field.

References

- ACI Committee 421, (1992). "Abstract of Shear Reinforcement for Slabs," *ACI Structural Journal,* Vol. 89, No. 5, pp 587-589.

- ACI Committee 363, (1992). "State-of-the-Art Report on High-Strength Concrete," *ACI 363R-92,* American Concrete Institute, Detroit.

- ACI Committee 318, (1983). "Building Code Requirements for Reinforced Concrete," (ACI 318-83), American Concrete Institute, Detroit, 111 pp.

- ACI Committee 318, (1989). "Building Code Requirements for Reinforced Concrete and Commentary," (ACI 318-89/318R-89), American Concrete Institute, Detroit, 353 pp.

- Agrawal, A.B. et al, (1976). "Crack propagation and Plasticity of Reinforced Concrete Shear-Wall Under Monotonic and Cyclic Loading," *Conference on Finite Element Methods in Engineering,* Adelaide, Australia.

- Agrawal, A.B. (1977). "Nonlinear Analysis if Reinforced Concrete Planar Structures Subject to Montonic, Reversed Cyclic and Dynarnic Loads," *Ph. D. Thesis,* University of New Brunswick, Fredericton, Canada.

- Alexander, S.D.B. and Simmonds, S.H. (1992). "Punching Shear Tests of Concrete Slab-Column Joints Containing Fiber Reinforcement," *ACI Structural Journal,* Vol. 89, No. 4. pp. 425-432.

126

- Al-Mahaidi, R.S.H. (1979). "Nonlinear Finite Element Analysis of Reinforced Concrete Deep Members," *Research Report No. 79-1*, Department of Structural Engineering, Cornell University, Ithaea, NY.

- Architectural Institute of Japan, (1988). "Standard for Structural Calculation of Reinforced Concrete Structures," Tokyo, pp. 106-109 (in Japanese).

- AS3600, (1988). "Australian Standard for Concrete Structures," Standard Association of Australia, North Sydney, 108 pp.

- ASCE, (1982). "Finite Element Analysis of Reinforced Concrete," New York, 545 pp.

- ASCE-ACI Joint Committee 426, (1974). "The Shear Strength of Reinforced Concrete Members-Slabs," *Journal of the Structural Division*, ASCE, Vol. 100, No. 8. pp. 1543-1591.

- ASTM (American Society for Testing and Materials), (1991a). "Standard Specification for Fly Ash and Raw or Calcined Natural Pozzolan for Use as a Mineral Admixture in Portland Cement Concrete" *(ASTM C 618-87) Annual Book of Standards*, V.04.02, Philadelphia.

- ASTM (American Society for Testing and Materials), (1991b). "Method of Making and Curing Concrete Test Specimens in the Laboratory," *(ASTM C 192-90a) Annual Book of Standards*, V.04.02, Philadelphia.

- ASTM (American Society for Testing and Materials), (1991c). "Test Method for Resistance of Concrete to Rapid Freezing and Thawing" *(ASTM C 666-90) Annual Book of Standards*, V.04.02, Philadelphia.

- ASTM (American Society for Testing and Materials), (1991d). "Test Method for Flexural Strength of Concrete Using Simple Beam with Third-point Loading" *(ASTM C 78-84) Annual Book of Standards*, V.04.02, Philadelphia.

- Bahlis, J.B. and Mirza, M.S. (1987). "Nonlinear Analysis of Planar Reinforced Concrete Structures," *Canadian Journal of Civil Engineering*, Vol. 14, pp. 771-779.

- Bashur, F.K. and Darwin, D. (1978). "Nonlinear Model for Reinforced Concrete Slabs," *Journal of Structural Division, ASCE*, Vol. 104, No. ST1.

- Bazant, Z.P., and Cao, Z. (1987). "Size Effect in Punching Shear Failure of Slabs," *ACI Structural Journal*, Vol. 84, No. 1, pp. 44-53.

- Bazant, Z.P., and Oh, B. H. (1983). "Cracking Band Theory for Fracture of Concrete," *Materials and Structures*, RILEM, 16(93), pp. 155-177.

- Bergan, P.G. and Holand, I. (1979). "Nonlinear Finite Element Analysis of Concrete Structures," *Computer Methods in Applied Mechanics and Engineering*, Vol. 17.

- BS 8110, (1985). "Structural Use of Concrete: Part 1, Code of Practice for Design and Construction," British Standards Institution, London, 126 pp.

- Broms, C.E. (1990). "Shear Reinforcement for Deflection Ductility of Flat Plates," *ACI Structural Journal*, Vol. 87, No. 6, pp. 696-705.

- Buyukozturk, O. (1977). "Nonlinear Analysis of Reinforced Concrete Structures," *Journal of Computers and Structures*, Vol. 7, February.

- Carrasquillo, Ramon L. et al. (1981). "Microcracking and Behavior of High-Strength Concrete Subject to Short-Term Loading," ACI Journal, *Proceedings* Vol. 78, No. 3. pp.179-186.

- Cedolin, L. and Dei Poli, S. (1977). "Finite Element Studies of Shear Critical Reinforced Concrete Beams," *Journal of the Engineering Mechanics Division, ASCE,* Vol. 103. No. EM3.

- Cervenka, V. and Gerstle, K.H. (1971). "Inelastic Analysis of Reinforced Concrete Panels," *Proceedings of International Association for Bridge and Structural Engineering,* Vol. 32-II.

- Chen, W.F. (1982). "Plasticity in Reinforced Concrete," McGraw-Hill, New York, 474 pp.

- Chen, Z. (1993). "Nonlinear Analysis of High-Strength Concrete Slabs," *M.Eng. thesis,* Memorial University of Newfoundland, St. John's, Newfoundland, Canada.

- Collins, M.P. et al. (1985). "An International Competition To Predict the Response of Reinforced Concrete Panels," *Canadian Journal of Civil Engineering,* Vol. 12, pp.624-644.

- Connor, J.J. and Sarne, Y. (1975). "Nonlinear Analysis of Prestressed Concrete Reactor Pressure Vessels," *Paper H2/2, 3rd International Conference on Structural Mechanics in Reactor Technology,* London.

- Corley, W.G. and Hawkins, N.M. (1968). "Shearhead Reinforcement for Slabs," *ACI Journal,* Vol. 65, No. 10. pp. 811-823.

- CSA A23.3-M84, (1984). "Code for the Design of Concrete Structures for Buildings," Canadian Standards Association, Rexdale, 281 pp.

- Darwin, D. and Pecknold, D.A. (1976). "Analysis of RC Shear Panels Under Cyclic Loading," *Journal of the Structural Division,* ASCE, Vol. 102, No. ST2.

- Dilger, W.H. and Ghali, A. (1981). "Shear Reinforcement for Concrete Slabs" *Journal of the Structural Division,* ASCE, Vol. 107, No. ST12. pp. 2403-2420.

- Elstner, R.C. and Hognestad, E. (1956). "Shearing Strength of Reinforced Concrete Slabs," ACI Journal, *Proceedings* Vol. 53, No. 1. pp. 29-58.

- Elgabry, A. and Ghali, A. (1990). "Design of Stud-Shear Reinforcement for Slabs," *ACI Structural Journal,* Vol. 87, No. 3. pp.350-361.

- Elwi, A.E. and Murray, D.W. (1984), "Nonlinear Analysis of reinforced and Prestressed Containments," *Proceedings of the International Conference on Computer-Aided Analysis and Design of Concrete Structures,* Part I, Split, Yugoslavia.

- Forsell, C. and Holemberg, A. (1946). "Concentrated Loads on Concrete Slabs," *Betong,* Vol. 31, No. 2, Stockholm, Sweden, pp. 95-123.

- Graf, O. (1938). "Strength Tests of Thick Reinforced Concrete Slabs Supported on All Sides Under Concentrated Loads," *Deutscher Ausschuss fur Eisenbeton,* No. 88, Berlin, Germany.

- Grootenboer, H.J. (1979). "Finite Element Analysis of Two Dimensional Reinforced Concrete Structures, Talking Account of nonlinear Physical Behaviour and the Development of Discrete Cracks," *Doctoral Disseertation,* Technical university of Delft, Holland.

• Gustafsson, P. and Hillerborg, A. (1988). "Sensitivity in Shear Strength of Longitudinally Reinforced Concrete Beams to Fracture Energy of Concrete," *ACI Structural Journal,* Vol. 85 No.3, pp. 286-294.

• Hand, F.R. et al, (1973). "Nonlinear Layered Analysis of RC Plates and Shells," *Journal of the Structural Division, ASCE,* Vol. 99, No. ST7.

• Hibbitt, H.D. et al, (1993). *ABAQUS,* HSK Corporation, Providence, R.I. V. 5.3

• Hognestad, E. (1953). "Shear Strength of Reinforced Concrete Column Footings," *Journal of the American Concrete Institute,* Vol. 50, No. 3. pp. 189-208.

• Hawkins, N. M. (1974a) "Shear Strength of Slabs with Shear Reinforcement," *Shear in Reinforced Concrete,* American Concrete Institute Special Publication, SP-42, pp. 785-816.

• Hawkins, N. M. (1974b) "Shear Strength of Slabs with Moments Transferred to Columns," *Shear in Reinforced Concrete,* American Concrete Institute Special Publication, SP-42, pp. 817-846.

• Jofrie' J.C., and McNiece, G.M. (1971). "Finite Element Analysis of Reinforced Concrete Slabs," *Journal of the Structural Division, ASCE,* Vol. 97, No. ST3.

• Kabir, A.F. and Scordelis, A.C. (1979). "Analysis of RC Shells for Time Dependent Effects," *IASS Bulletin,* No. 69.

• Langohr, H. et al. (1976). "Special Shear Reinforcement for Concrete Flat Plates," ACI Journal, *Proceedings* Vol. 73, No. 3. pp. 141-146.

• Lin, C.S. and Scordelis, A.C. (1975). "Nonlinear Analysis of RC Shells of General Form," *Journal of Structural Division, ASCE,* Vol. 101, No. ST3.

• Maage, M. and Helland, S. (1991). "Quality Inspection of 'Shore Approach' High-Strength Concrete," *ACI Special Publication,* SP-126, pp. 609-629.

• Malhotra, V. et al. (1988) "Current Status of CANMET's Studies on the Durability of Concrete Containing Supplementary Cementing Materials in Marine Environment," *ACI Special Publication,* SP-109, pp. 31-72.

• Marzouk, H. and Chen, Z. (1993). "Finite Element Analysis Of High-Strength Concrete Slabs" *ACI Structural Journal,* V. 90, No. 5, pp. 505-513.

• Marzouk, H. and Hussein, A. (1989). "Development of 70MPa Concrete for the Nekton Project Using Local Available Materials in Newfoundland," *Ocean Engineering Research Group,* Memorial University of Newfoundland, St. John's, Newfoundland, Canada, pp. 146.

• Marzouk, H. and Hussein, A. (1990). "Properties of high-Strength Concrete at Low Temperatures," *ACI Materials Journal,* Vol. 87, No. 2. pp. 167-171.

• Marzouk, H. and Hussein, A. (1991). "Experimantal Investigation on the Behaviour of High-Strength Concrete Slabs," *ACI Structural Journal,* Vol. 88, No. 6. pp. 701-713.

• Marzouk, H. and Jiang, D. (1993a). "Punching Shear Behaviour of High-Strength Concrete Slabs," *Proceedings of the Canadian Society for Civil Engineering Annual Conference (1993),* pp. 523-531.

- Marzouk, H. and Jiang, D. (1993b). "The Effects of Freezing and Thawing on the Tension Properties of High-Strength Concrete," Accepted by *ACI Materials Journal*.

- Massicotte, B. Elwi, A.E. and MacGregor, J. G. (1990). "Tension Stiffening Model for Planar Reinforced Concrete Members," *Journal of Structural Division, ASCE*, Vol. 116, No. 11, pp. 3039-3058.

- Mehta, P.K. (1991). "Durability of Concrete-Fifty Years of Progress ?" *ACI Special Publication*, SP-126, pp. 1-30.

- Mokhtar, A.S. et al. (1986). "Stud Shear Reinforcement for Flat Concrete plates," *ACI Structural Journal*, Vol. 82, No. 5. pp. 676-683.

- Mortin, J.D. and Ghali, A. (1991). "Connection of Flat Plates to Edge Columns," *ACI Structural Journal*, Vol. 88, No. 2. pp. 192-198.

- Ngo, D. and Scordelis, A.C., (1967). "Finite Element Analysis of Reinforced Concrete Beams," *ACI Structural Journal*, Vol. 64, No. 3.

- Regan, P.E. (1984). "Dependance of punching Resistance upon the geometry of the Failure Surface," *Magazine of Concrete Research*, Vol. 36, No. 126. pp. 3-8.

- Richart, F.E. and Kluge, R. W. (1939). "Tests of Reinforced Slabs Subjected to Concentrated Loads," *Bulletin 314*, University of Illinois, Engineering Experiment Station.

- Seible, F. et al. (1980). "Preassembled Shear Reinforcement Units for Flat Plates," *ACI Structural Journal*, Vol. 77, No. 1. pp. 28-35.

- Shah, S.P. et al. (1981). "An Experimental Technique for obtaining Complete Stress-Strain Curves for High-Strength Concrete," *Cement, Concrete and Aggregates*, Vol. 3, No. 1, pp. 21-27.

- Schnobrich, W.C. (1974). "Finite Element Determination of Nonlinear Behaviour of Reinforced Concrete Plates and Shells," *Proceedings of the Symposium on Nonlinear Techniques and Behaviour in Structural Analysis*, Transport and Road Research Laboratory, Department of Enviroment, United Kingdom

- Schnobrich, W.C. (1977). "Behaviour of Reinforced Concrete Concrete Structures Predicted by the Finite Element Method," *Computers and Structures*, Vol. 7.

- Schnobrich, W.C. (1978). "Finite Element Analysis of Reinforced Concrete Structures," Chapters B4 - Slabs, Cl - Panels and Walls, C2 - Shells, *Symposium on Analysis of Reinforced Concrete Structures by the Finite Element Method*, Politechnico Di Milan, Italy.

- Scordelis, A.C., (1972). "Finite Element Analysis of Reinforced Concrete Structures," *Proceedings of the Specialty Conference on Finite Element Method in Civil Engineering*, Montreal, Quebec, Canada.

- Scordelis, A.C., (1978). "Finite Element Analysis of Reinforced Concrete Structures," Chapters Bl - Modeling, B3 - Beams, C3 - Frames, C4 - Segmental Bridges, *Symposium on Analysis of Reinforced Concrete Structures by the Finite Element Method*, Politechnico Di Milan, Italy.

- Shah, S.P. (1981b). "High Strength Concrete–A Workshop Summary," *Concrete International: Design & Construction*, Vol. 3, No. 5, pp. 94-98.

- Shareef, S.S. and Buyukozturk, O. (1983). "Constitutive Modeling of Concrete in Finite Element Analysis," *Research Report No. R83-16,* Department of Civil Engineering, Massachusetts Institute of Technology, Cambridge, MA.

- Tasuji, M.E. et al. (1976). "The Behaviour of Plain Concrete Subjected to Biaxial Stresses," *Report No. 360,* Departmant of Structural Engineering, Cornell University, Ithaca, NY.

- Vanderbilt, M.D. (1972). "Shear Strength of Continuous Plates," *Journal of the Structural Division,* ASCE, Vol. 98, no. 5. pp. 961-973.

- Van Dusen, M. H., (1985). "Unbalanced Moment and Shear Transfer at Slab-Column Connections: A Literature Review," *M.Eng. thesis,* University of Toronto, 126 pp.

- Vecchio, F., and Collins, M.P. (1982). "The Response of Reinforced Concrete to In-Plane Shear Stresses," *Research Report,* Department of Civil Engineering, University of Toronto, Toronto, Ont.

- Wang, P.T.; Shah, S.P.; and Naaman, A.E. (1978). "Stress-Strain Curves of Normal and Lightweight Concrete in Compression," ACI Journal, *Proceedings* Vol.75, No. 10, pp. 603-601.

- Wegner, R., (1976). "Finite Element Models for Reinforced Concrete," Preprint, Proceedings, *U.S.-Germany Symposium,* M.I.T., Boston.

- Whiting, D. and Burg, R., (1991). "Freezing and Thawing Durability of High-Strength Lightweight Concretes," *ACI Special Publication,* SP-126, pp. 83-100.

- Yamada, T. et al. (1992). "Punching Shear Resistance of Flat Slabs: Influence of Reinforcement Type and Ratio," *ACI Structural Journal*, Vol. 89, No. 5. pp. 555-562.

- Zienkiewicz, O.C. et al, (1971). "Finite Element Method in Analysis of Reinforced and Prestressed Concrete Structures," *Paper M1/1, 1st International Conference on Structural Mechanics in Reactor Technology*, Vol. 20.